
Phase-driven Domain Generalizable Learning for Nonstationary Time Series

Payal Mohapatra^{*1} Lixu Wang^{*1} Qi Zhu¹

Abstract

Monitoring and recognizing patterns in continuous sensing data is crucial for many practical applications. These real-world time-series data are often *nonstationary*, characterized by varying statistical and spectral properties over time. This poses a significant challenge in developing learning models that can effectively generalize across different distributions. In this work, based on our observation that nonstationary statistics are intrinsically linked to the phase information, we propose a time-series learning framework, PhASER. It consists of three novel elements: 1) phase augmentation that diversifies non-stationarity while preserving discriminatory semantics, 2) separate feature encoding by viewing time-varying magnitude and phase as independent modalities, and 3) feature broadcasting by incorporating phase with a novel residual connection for inherent regularization to enhance distribution invariant learning. Upon extensive evaluation on 5 datasets from human activity recognition, sleep-stage classification, and gesture recognition against 10 state-of-the-art baseline methods, we demonstrate that PhASER consistently outperforms the best baselines by an average of 5% and up to 13% in some cases. Moreover, PhASER’s principles can be applied broadly to boost the generalization ability of existing time series classification models.

1. Introduction

Time-series data play a ubiquitous and crucial role in numerous real-world applications, such as continuous monitoring for human activity recognition (Li et al., 2020), gesture identification (Ozdemir et al., 2020), sleep tracking (Kemp et al., 2000), and more. The collected continuous time series often exhibit *non-stationarity*, i.e., the statistical and spectral properties of the data evolve over time. Another inherent challenge is the distribution shift due to the underlying

sensing properties or subject-specific attributes, commonly referred to as *domain shift*, which directly impacts the performance of time-series models. Thus, it is imperative to develop methods for more generalizable pattern recognition in nonstationary time series.

Some past methods (Ragab et al., 2023a;b; He et al., 2023b) address distribution shifts in time-series applications by accessing target domain samples through domain adaptation algorithms. However, accessing data from unseen distributions in advance may not be possible in practice. To overcome this challenge, a few works (Gagnon-Audet et al., 2022; Xu et al., 2022) applied standard domain generalization (DG) algorithms (Volpi et al., 2018; Sagawa et al., 2019; Parascandolo et al., 2020) to temporally-changing time-series data, but reported a significant performance gap when compared with visual data. Recent research on DG tailored for time series has been exploring promising directions like latent-domain characterization (Lu et al., 2023; Du et al., 2021), augmentation strategies (Iwana & Uchida, 2021; Li et al., 2021), preservation of non-stationarity dictionary (Liu et al., 2022b; Kim et al., 2021c), and leveraging spectral characteristics of time series (He et al., 2023a; Yang & Hong, 2022; Kim et al., 2021a). Although these methods have shown success in certain cases, they still suffer from various limitations. Latent-domain characterization is heavily reliant on their hypotheses of latent domains, which limits its broader applicability. Augmentation strategies (shift, jittering, masking, etc.) for time-series data have restricted utility (Iwana & Uchida, 2021). For instance, in physiological signal analysis, morphological alterations through augmentations are detrimental, and time-slicing is unsuitable for periodic signals. Moreover, advanced augmentation techniques, like spectral perturbations (time-frequency warping, decomposition techniques, etc.) are usually heavily parametric (Wen et al., 2020) and application-specific. Approaches based on preserving non-stationarity are constrained by the need for encoders to maintain the same input-output space, which is limiting, especially for classification tasks. Although a few works (He et al., 2023a; Yang & Hong, 2022) emphasize frequency domain representations where robustness to feature shifts is central, they don’t consider cases where the spectral response is time-varying. Another significant issue is that many of these studies rely on domain identity, which in practice can be expensive and intrusive to

^{*}Equal contribution ¹Northwestern University, Evanston, IL, USA. Correspondence to: Qi Zhu <qzhu@northwestern.edu>.

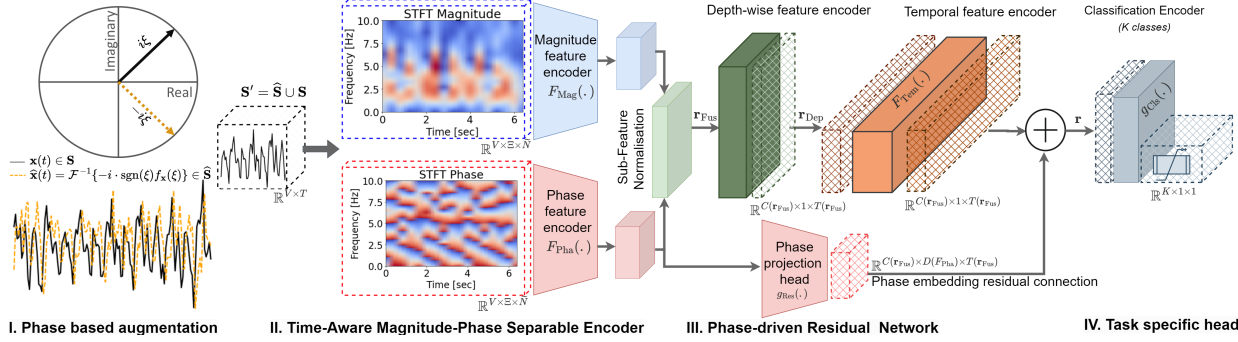


Figure 1. Overview of PhASER and its four components. I. illustrates the phase-based augmentation using a phasor representation (top left) for the negative and positive frequency components of a signal. The augmentation translates a signal to its $\pi/2$ phase-shifted version. II. demonstrates the separate encoders for time-varying magnitude and phase responses with sub-feature normalization. III. shows the phase-driven residual network with dimensions of the intermediate feature map. IV. is the task-specific classification head.

obtain, especially in healthcare and finance (Yan et al., 2024; Bai et al., 2022). Hence, achieving domain-generalizable time series classification without access to unseen distributions and domain labels of available distributions remains a challenging yet crucial pursuit.

Our Approach and Contributions. In this work, we aim to achieve domain-generalizable learning for time series in real-world scenarios that are persistently time-varying or *nonstationary*. By leveraging the phase information of time series, we propose a novel Phase-Augmented Separate Encoding and Residual (PhASER) framework. There are three key modules in PhASER. First, PhASER can diversify the non-stationarity of source domain data through an intra-instance phase shift. Favorably, using Hilbert Transform (HT) (King, 2009) to conduct a phase-shift-based augmentation overcomes the shortcomings of existing techniques by being general and non-parametric. Next, PhASER applies a less-explored strategy – taking time-varying magnitude and phase responses of the frequency domain as separate inputs, to better integrate the time-frequency information. Finally, we design an effective broadcasting mechanism with a non-linear residual connection between the phase-encoded embedding and the backbone representation. In this way, PhASER can benefit from the inherent regularization (He et al., 2020; Marion et al., 2023) to learn domain-invariant features while offsetting any degradation to the desirable underlying representation (He et al., 2016). An overview of PhASER is illustrated in Figure 1. The details of PhASER are presented in Section 2, where we also theoretically substantiate our design philosophy by demonstrating the importance of addressing non-stationarity in optimizing classification risks of unseen distributions and the role of HT in changing nonstationary statistics of time series. In Section 3, we conduct extensive experiments on 5 benchmark datasets across 3 popular application scenarios and demonstrate the superior performance of PhASER over a comprehensive set of state-of-the-art approaches. We also validate the effectiveness of each component in PhASER

and its general applicability through systematic analysis. Section 4 discusses additional related works beyond those mentioned in introduction. Section 5 concludes the paper.

2. Approach

2.1. Problem Formulation

Definition 2.1 (Nonstationary Time Series). Following the definition of mixed decomposition in Dama & Sinoquet (2021), we assume a continuous time-series sample drawn from a nonstationary domain $\mathbf{x} = \{x_0, \dots, x_t, \dots\} \sim \mathcal{D}_{\mathbf{x}}$ can be decomposed into components with mean μ_t and variance σ_t (both μ_t and σ_t are not always zero),

$$\Pr_{\mathbf{x} \sim \mathcal{D}_{\mathbf{x}}}(\mathbf{x})(t) = \mu_t + \sigma_t \times z, \quad (1)$$

$$\forall L \geq 1, \exists t, [\mu_t \neq \mu_{t+L}] \vee [\sigma_t \neq \sigma_{t+L}],$$

where z is a stationary stochastic component with a zero mean and a unit variance.

Definition 2.2 (Time Series Domain Generalization). Suppose there is a dataset $\mathbf{S} = \{(\mathbf{x}_i, y_i)\}_{i=1}^M$ with M data samples drawn from a set of N_S nonstationary source domains $\mathcal{S} = \{\mathcal{S}_i\}_{i=1}^{N_S}$. The joint distribution of \mathbf{S} is $\Pr(\mathcal{X}_{\mathcal{S}}, \mathcal{Y}_{\mathcal{S}})$, i.e., $\mathbf{x}_i \sim \mathcal{X}_{\mathcal{S}}, y_i \sim \mathcal{Y}_{\mathcal{S}}$ and $\mathbf{x}_i \in \mathbb{R}^{V \times T}$ where V is the number of time series feature dimensions and T is the sequence length. $y_i \in \mathbb{R}^{1 \times 1}$ is the categorical label. Note that the joint distributions of different source domains are similar but distinct,

$$\Pr(\mathcal{X}_{\mathcal{S}_i}, \mathcal{Y}_{\mathcal{S}_i}) \neq \Pr(\mathcal{X}_{\mathcal{S}_j}, \mathcal{Y}_{\mathcal{S}_j}), 1 < i \neq j \leq N_S. \quad (2)$$

For any potential unseen target domain \mathcal{D}_U , its joint distribution remains distinct like Eq. (2). In our problem, although the source dataset is assumed to contain multiple domains, the annotations that specify the domain identity are unavailable. Our goal is to train a model consisting of a feature extractor F and a classifier g using the given source dataset ($F \circ g : \mathcal{X}_{\mathcal{S}} \rightarrow \mathcal{Y}_{\mathcal{S}}$), such that

$$\min_{(\mathbf{x}, y) \sim \mathcal{D}_U} \mathbb{E} [\mathcal{L}(g(F(\mathbf{x})), y)], \quad (3)$$

where $\mathcal{L}(\cdot)$ is a certain cost that measures the errors between model predictions and the ground-truth labels.

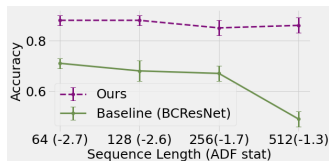


Figure 2. Performance comparison between PhASER (Ours) and BCResNet with increasingly nonstationary HHAR dataset.

Input Modality	Accuracy
Only Mag	0.81 \pm 0.03
Only Pha	0.62 \pm 0.03
Mag-Pha Concatenate	0.73 \pm 0.03
Mag-Pha Separate	0.85 \pm 0.01

Table 1. Performance comparison of various input configurations for time-frequency information.

Motivation. We start by providing a motivation example on a human activity recognition (HAR) application where non-stationarity is unavoidable due to user’s behavioral changes or sensor characteristics (Bangaru et al., 2020). The central question is: *What is the impact of the non-stationarity of time series on models’ generalization ability?* We create a simple empirical study on a dataset called HHAR (Stisen et al., 2015) and update the sequence length to build various levels of non-stationarity, which is measured by the Augmented Dickey-Fuller (ADF) statistics (a higher ADF value indicates greater non-stationarity). More details of the ADF test are given in Section B of Appendix. We adopt a popular DG model for time series classification – BCResNet (Kim et al., 2021a), to explore the relation between the degree of non-stationarity and the model’s generalization ability to unseen domains. Figure 2 shows a clear decreasing trend in the accuracy of BCResNet as the non-stationarity increases, highlighting the *importance of addressing non-stationarity for achieving better generalization*. In contrast, our proposed PhASER framework, as detailed below, consistently performs well despite increasing non-stationarity.

Overview of PhASER. As shown in Figure 1, the proposed Phase-Augmented Separate Encoding and Residual framework (PhASER) begins with an augmentation module that utilizes the Hilbert Transform to generate out-of-phase augmentations for time series. These augmentations not only diversify non-stationarity but also preserve category-discriminatory semantics. Next, the short-term Fourier Transform (STFT) is employed to obtain temporal magnitude and phase responses. Two separate encoders then process the magnitude and phase as distinct input modalities. Finally, PhASER establishes a novel feature broadcasting mechanism to incorporate the phase information deeper in the layers through residual connections. By emphasizing the phase, the PhASER framework implicitly regularizes the representations against non-stationarity and offsets any degradation to the desirable features. Consequently, the classifier can learn domain-agnostic task-discriminatory representations. In the following Sections 2.2 to 2.4, we will introduce the details of these three novel elements in PhASER, and then discuss the theoretical insights in Section 2.5.

2.2. Hilbert Transform based Phase Augmentation

Our motivating study depicted in Figure 2, demonstrates the importance of addressing non-stationarity to enhance the generalization ability of models. An intuitive technique is to leverage data augmentation to diversify the non-stationarity of training data. The optimal augmentation also needs to preserve the discriminatory properties of the original data, which is essential to differentiate semantic categories.

Different from existing time series augmentation techniques, we choose to introduce a phase shift in a signal while preserving the magnitude response, thereby offering an augmented view. As it is a less-studied technique, we intuitively justify our design choice by studying the question: *Does shifting the phase of time series spectral response change its non-stationarity?* Figure 3 (a) visualizes a univariate accelerometer data sample from HHAR in the time domain to illustrate its non-stationarity. If we segment this sample into sequential windows and conduct Discrete Fourier Transform (DFT) to obtain its magnitude and phase responses as plotted in Figure 3 (b) and (c), we can observe the shift in the spectral domain corresponding to non-stationarity. Figure 3 (d) depicts a time-series sample produced by phase-shifting its original sample, and we can observe evident changes in the non-stationarity statistics.

Following our observations from Figure 3, to diversify the non-stationarity and preserve discriminatory features, we propose a simple but effective data augmentation technique based on the Hilbert Transform (HT). Specifically, for each time-series sample \mathbf{x} in the source dataset \mathbf{S} , we can assume it is a real-valued signal $\mathbf{x} = \{x_0, \dots, x_t, \dots\} \in \mathbb{R}$ that is characterized by the deterministic function $x_t = \mathbf{x}(t)$. Then, $\text{HT}(\mathbf{x}(t)) = \hat{\mathbf{x}}(t) = \int_{-\infty}^{\infty} \mathbf{x}(\tau) \frac{1}{\pi(t-\tau)} d\tau$. HT can be easily interpreted in the frequency domain via Fourier analysis,

$$f_{\mathbf{x}}(\xi) = \mathcal{F}\{\mathbf{x}(t)\} = \int_{-\infty}^{\infty} \mathbf{x}(t) e^{i2\pi\xi t} dt, -\infty < \xi < \infty,$$

$$\mathbf{x}(t) = \mathcal{F}^{-1}\{f_{\mathbf{x}}(\xi)\} = \int_{-\infty}^{\infty} f_{\mathbf{x}}(\xi) e^{i2\pi\xi t} d\xi, -\infty < t < \infty,$$

where \mathcal{F} , \mathcal{F}^{-1} denote the Fourier transform and inverse, and ξ is the frequency variable. To interpret $\hat{\mathbf{x}}$ in the frequency domain, the negative frequency spectrum of $f_{\mathbf{x}}(\xi)$ needs to multiply with the imaginary unit i , while the positive spectrum needs to multiply with $-i$. Then we have,

$$\text{HT}(\mathbf{x}(t)) = \hat{\mathbf{x}}(t) = \mathcal{F}^{-1}\{-i \cdot \text{sgn}(\xi) f_{\mathbf{x}}(\xi)\}, \quad (4)$$

where $\text{sgn}(\cdot)$ is a sign function. Applying HT on a signal results in a phase shift of $\pi/2$, yielding a new out-of-phase signal. After obtaining the transformed $\hat{\mathbf{x}}$ for all feature dimensions of all samples, we merge the augmented dataset $\hat{\mathbf{S}}$ and the original \mathbf{S} to form a new larger dataset $\mathbf{S}' = \hat{\mathbf{S}} \cup \mathbf{S}$. For the following design, there is no distinction among the samples in \mathbf{S}' , based on whether they belong to $\hat{\mathbf{S}}$ or \mathbf{S} .

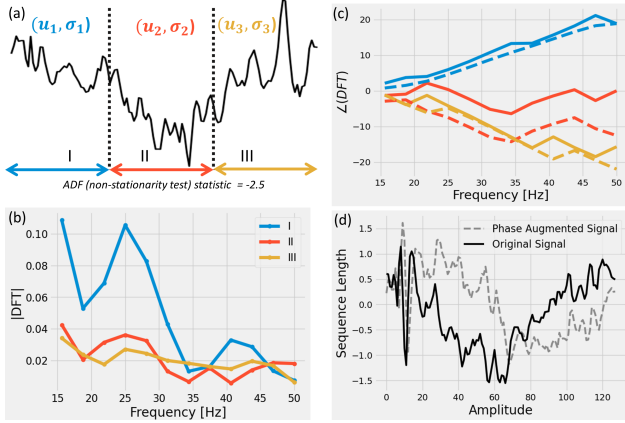


Figure 3. Illustrating example of diversification of non-stationarity by shifting the phase of a signal. (a) Temporal non-stationarity in a time-series data with varying mean (μ) and variance (σ) within a domain. (b) Magnitude response of the Discrete Fourier Transform (DFT) of each region. Highlights shift in the dominant frequencies. (c) Original and shifted phase responses for each region. (d) Corresponding time series using phase-based augmentation.

2.3. Magnitude-Phase Separate Encoding

After augmenting the source domain with phase-shift using HT, next, we identify optimal ways to encode time series for generalization. While employing spectral transformation is a common approach, our perspective diverges from most existing studies which typically view time and frequency separately. Instead, we unify the time and frequency context and consider the magnitude and phase information as distinct modalities of the original signals.

As we address the non-stationarity of time series, we adopt STFT rather than DFT. DFT is usually applicable to signals that are stationary and periodic over time, and not suitable for analyzing time-varying signals. STFT is obtained by applying DFT sequentially with a specified window through the entire length of the time series. Specifically, for each training sample $\mathbf{x} \in \mathbf{S}'$ with a continuous time function $\mathbf{x}(t)$, sampling it at a fixed rate generates a discrete time series denoted as $\mathbf{x}[n]$ with a sequence length N , we have,

$$f_{\mathbf{x}}[n, k] = \sum_{m=n-(W-1)}^n w[n-m] \mathbf{x}[m] e^{i\xi_k m}. \quad (5)$$

The STFT of $\mathbf{x}[n]$, $f_{\mathbf{x}}[n, k]$, is a function of both discrete time n and frequency bin indices k with lengths \tilde{N} and Ξ , respectively. ξ_k is a digital frequency variable given by $\xi_k = \frac{2\pi k}{\Xi}$ and $w[\cdot]$ is a window function. Without losing generality, we adopt a commonly used Hanning window with window length W , i.e., $w[n] = 0.5(1 - \cos \frac{2\pi n}{W-1})$ where $0 \leq n \leq W-1$. Note that the length and shape of the window determine the time-frequency resolution. A larger W provides better frequency resolution and a smaller W gives a better temporal scale. We set W to be randomly sampled powers of 2 for each time series feature dimension,

i.e., $W_i = 2^{p_i} \leq \Xi, p_i \sim \mathcal{U} \in \mathbb{Z}_0^+, i \in [1, V]$ where \mathcal{U} denotes a uniform distribution for integers. After obtaining $f_{\mathbf{x}}[n, k]$, we can compute its magnitude and phase as,

$$\begin{aligned} \text{Mag}(\mathbf{x}) &= \sqrt{\text{Re}(f_{\mathbf{x}}[n, k])^2 + \text{Im}(f_{\mathbf{x}}[n, k])^2}, \\ \text{Pha}(\mathbf{x}) &= \arctan 2(\text{Im}(f_{\mathbf{x}}[n, k]), \text{Re}(f_{\mathbf{x}}[n, k])), \end{aligned} \quad (6)$$

where $\text{Im}(\cdot)$ and $\text{Re}(\cdot)$ indicate imaginary and real parts of a complex number, and $\arctan 2(\cdot)$ is the two-argument form of \arctan . Then we take $\text{Mag}(\mathbf{x}), \text{Pha}(\mathbf{x}) \in \mathbb{R}^{V \times \Xi \times \tilde{N}}$ as inputs of two separate encoders F_{Mag} and F_{Pha} , respectively. The merit of this strategy is based on the ability to fully reconstruct a time-series signal solely using phase and magnitude response (Hayes et al., 1980; Jacques & Feuillen, 2020). We also support this choice with an intuitive study.

Intuition of treating phase and magnitude as separate modalities. Combining insights from past works (He et al., 2023a; Kim et al., 2021a; Mohapatra et al., 2023b) that have underscored the value of using spectral input for generalizable learning, along with non-stationarity in time-series applications, we conduct a small-scale empirical study on an HAR dataset – WISDM (Kwapisz et al., 2011), to determine the optimal input way of time-frequency information. Note that for the time-frequency representation, STFT is applied to obtain the magnitude and phase responses. We experiment with four choices of time-frequency inputs: 1) magnitude-only input, 2) phase-only input, 3) concatenate magnitude and phase, and 4) separate encoders for magnitude and phase, under identical evaluation settings. Table 1 in the previous page shows that using only the phase input performs much worse than using only magnitude, which implies that magnitude response contains more semantic-discriminatory information. However, we can also observe that simply concatenating both the phase and magnitude cannot boost the performance, while separately encoding magnitude and phase followed by a late fusion is a superior choice. This may be attributed to 1) the independent selection of high-level features from the magnitude and phase for the task of classification, and 2) the learning about non-stationarity from the phase.

Before fusing the extracted embeddings of F_{Mag} and F_{Pha} , we incorporate sub-feature normalization to isolate low and high-frequency information to overcome domain-specific attributes (e.g., steady-state drifts arising due to domain, device or stimuli, differences) (Phaye et al., 2019; Chang et al., 2021). Specifically, the embeddings of F_{Mag} and F_{Pha} are divided into B sub-feature spaces. We apply normalization in each sub-feature space for each time series variate,

$$F_{\text{Mag}}(\mathbf{x}) = \left\{ F_{\text{Mag}}(\mathbf{x})_b := \frac{F_{\text{Mag}}(\mathbf{x})_b - \overline{F_{\text{Mag}}(\mathbf{x})_b}}{\sigma(F_{\text{Mag}}(\mathbf{x})_b)} \right\}_{b=1}^B,$$

where $\overline{(\cdot)}$ and $\sigma(\cdot)$ denote to compute the mean and variance of the given input. The same sub-feature normalization

is also conducted on $F_{\text{Pha}}(\mathbf{x})$. Then, both $F_{\text{Mag}}(\mathbf{x})$ and $F_{\text{Pha}}(\mathbf{x})$ are fused along the variate axis by multiplying with 2D convolution kernels denoted as a fusing encoder F_{Fus} . The fused embeddings $\mathbf{r}_{\text{Fus}} = F_{\text{Fus}}(F_{\text{Mag}}(\mathbf{x}), F_{\text{Pha}}(\mathbf{x}))$ are then fed into the following modules.

2.4. Phase-Residual Feature Broadcasting

Lastly, we outline our approach to achieve domain generalizable representation learning via a phase-based broadcasting technique. It starts with a depthwise feature encoder, F_{Dep} , which transforms the fused embeddings, \mathbf{r}_{Fus} , into 1D feature maps, \mathbf{r}_{Dep} , along the temporal dimension, given as,

$$\mathbb{R}^{C(\mathbf{r}_{\text{Fus}}) \times D(\mathbf{r}_{\text{Fus}}) \times T(\mathbf{r}_{\text{Fus}})} \rightarrow \mathbb{R}^{C(\mathbf{r}_{\text{Fus}}) \times 1 \times T(\mathbf{r}_{\text{Fus}})},$$

where $C(\cdot)$, $D(\cdot)$, and $T(\cdot)$ represent the channel number, the feature dimensions, and the temporal dimensions of an embedding. F_{Dep} is implemented as several convolution layers followed by an average pooling operation to unify all features at each temporal index. Once the 1D feature map is obtained, we attach a sequence-to-sequence (the dimension format of the feature map remains intact) temporal encoder, F_{Tem} , to characterize its temporal dependency and semantics. The choice of backbone for F_{Tem} is not central to our design and a suitable sequence-to-sequence encoder can be chosen. Here we leverage convolution layers to form F_{Tem} , and we have also tested other architectures (please refer to Section B in Appendix for details). We adopt this feature consolidation approach to enable specialized learning of spectral attributes by F_{Dep} and global temporal dependencies using F_{Tem} , resulting in a more valuable overall semantic characterization.

Note that after a series of operations, like fusing and dimension reduction, the non-stationarity degrades gradually. To counteract such degradation, we introduce a non-linear projection of $F_{\text{Pha}}(\mathbf{x})$ as a shortcut through F_{Dep} to F_{Tem} . Building on our previous steps of diversifying non-stationarity and preserving semantic attributes, this residual connection ensures the learning of distribution-shift-invariant representations through inherent regularization. To suitably broadcast with the output dimensions of F_{Tem} , we use a projection head, g_{Res} for the transformation,

$$\begin{aligned} & \mathbb{R}^{C(F_{\text{Pha}}(\mathbf{x})) \times D(F_{\text{Pha}}(\mathbf{x})) \times T(F_{\text{Pha}}(\mathbf{x}))} \\ & \rightarrow \mathbb{R}^{C(\mathbf{r}_{\text{Fus}}) \times D(F_{\text{Pha}}(\mathbf{x})) \times T(\mathbf{r}_{\text{Fus}})}. \end{aligned}$$

After the projection, we can broadcast the output of F_{Tem} to form the final representation \mathbf{r} that is intended to learn discriminatory characteristics despite non-stationarity. Overall, the broadcasting can be expressed as

$$\mathbf{r} = F_{\text{Tem}}(\mathbf{r}_{\text{Dep}}) + g_{\text{Res}}(F_{\text{Pha}}(\text{Pha}(\mathbf{x}))) \quad (7)$$

After considerable efforts to preserve and enhance the discriminatory characteristics amid input's non-stationarity, we

finally optimize for semantic distinction. This optimization is easily achieved with CrossEntropy Loss applied to a simple classification head, g_{Cls} , attached to F_{Tem} given as,

$$\mathcal{L}_{\text{CE}} = \frac{1}{N_B} \sum_{i=1}^{N_B} \mathbf{y}_i \log g_{\text{Cls}}(\mathbf{r}), \quad (8)$$

where N_B is the size of a batch in the mini-batch training, and \mathbf{y}_i is the one-hot form of the label y_i .

2.5. Theoretical Insights

Here we provide some theoretical insights to demonstrate that our method design is rigorously motivated. Detailed relevant definitions and proofs of the following theorems and lemmas are provided in Section A of Appendix.

Definition 2.3 (β -Divergence). Suppose two data domains $\mathcal{D}_1, \mathcal{D}_2$ are built on input variable \mathbf{x} and label variable y . Let $q > 0$ be a constant, the β -Divergence between \mathcal{D}_1 and \mathcal{D}_2 is defined as

$$\beta_q(\mathcal{D}_1 \parallel \mathcal{D}_2) = \left[\mathbb{E}_{(\mathbf{x}, y) \sim \mathcal{D}_2} \left(\frac{\mathcal{D}_1(\mathbf{x}, y)}{\mathcal{D}_2(\mathbf{x}, y)} \right)^q \right]^{\frac{1}{q}}. \quad (9)$$

According to the definition in Germain et al. (2016), β -Divergence can be linked to Rényi Divergence (Van Erven & Harremos, 2014) $\text{RD}_q(\cdot)$ as

$$\beta_q(\mathcal{D}_1 \parallel \mathcal{D}_2) = 2^{\frac{q-1}{q} \text{RD}_q(\mathcal{D}_1 \parallel \mathcal{D}_2)}. \quad (10)$$

Lemma 2.4 (Bounding β -Divergence in A Convex Hull).

Let S be a set of source domains, denoted as $S = \{\mathcal{S}_i\}_{i=1}^{N_S}$. A convex hull Λ_S considered here consists of a mixture distributions $\Lambda_S = \{\bar{\mathcal{S}} : \bar{\mathcal{S}}(\cdot) = \sum_{i=1}^{N_S} \pi_i \mathcal{S}_i(\cdot), \pi_i \in \Delta_{N_S-1}\}$, where Δ_{N_S-1} is the $N_S - 1$ -th dimensional simplex. Let $\beta_q(\mathcal{S}_i \parallel \mathcal{S}_j) \leq \epsilon$ for $\forall i, j \in [N_S]$, then we have the following relation for the β -Divergence between any pair of two domains $\mathcal{D}', \mathcal{D}'' \in \Lambda_S$ in the convex hull,

$$\beta_q(\mathcal{D}' \parallel \mathcal{D}'') \leq \epsilon. \quad (11)$$

Theorem 2.5 (Risk of An Unseen Time series Domain).

Let \mathcal{H} be a hypothesis space built from a set of source time series domains, denoted as $S = \{\mathcal{S}_i\}_{i=1}^{N_S}$ with the same value range (i.e., the supports of these source domains are the same). Suppose $q > 0$ is a constant, for any unseen time series domain \mathcal{D}_U from the convex hull Λ_S , we have its closest element $\mathcal{D}_{\bar{U}}$ in Λ_S , i.e., $\mathcal{D}_{\bar{U}} = \arg \min_{\pi_1, \dots, \pi_{N_S}} \beta_q(\mathcal{D}_{\bar{U}} \parallel \sum_{i=1}^{N_S} \pi_i \mathcal{S}_i)$. Then the risk of \mathcal{D}_U on any ρ in \mathcal{H} is,

$$R_{\mathcal{D}_U}[\rho] \leq \frac{1}{2} d_{\mathcal{D}_U}(\rho) + \epsilon \cdot [e_{\mathcal{D}_{\bar{U}}}(\rho)]^{1-\frac{1}{q}}, \quad (12)$$

where $d_{\mathcal{D}}(\rho)$ and $e_{\mathcal{D}}(\rho)$ are an expected disagreement and an expected joint error of a domain \mathcal{D} , respectively. The ϵ is a value larger than the maximum β -Divergence in Λ_S ,

$$\epsilon \geq \max_{i, j \in [N_S], i \neq j, t \in [0, +\infty)} 2^{\frac{q-1}{q} \text{RD}_q(\mathcal{S}_i(t) \parallel \mathcal{S}_j(t))}, \quad (13)$$

$$\text{where } \text{RD}_q(\mathcal{S}_i(t) \parallel \mathcal{S}_j(t)) = \frac{q(\mu_{j,t} - \mu_{i,t})^2}{2(1-q)\sigma_{i,t}^2 + 2\sigma_{j,t}^2} + \frac{\ln \frac{\sqrt{(1-q)\sigma_{i,t}^2 + \sigma_{j,t}^2}}{\sigma_{i,t}^{1-q}\sigma_{j,t}^q}}{1-q}}{1-q}. \quad (14)$$

Insights. Theorem 2.5 indicates the optimization directions for reducing the generalization risk of an unseen target domain. According to Eq. (12), the risk is bounded by two terms. However, our efforts can be focused solely on the second term. The first term $d_{\mathcal{D}_U}(\rho)$ is the expected disagreement of \mathcal{D}_U and we are unable to conduct any approximation without access to the data from \mathcal{D}_U . Regarding the second term, the coefficient ϵ can be viewed as the maximum β -Divergence of source domains, and thus we should design a method to minimize the β -Divergence. Moreover, according to Eq. (14), the nonstationary statistics of time series are arguments of the β -Divergence, which validates the importance of addressing non-stationarity if we want to minimize the domain discrepancy. Besides, $e_{\mathcal{D}_U}(\rho)$ tells us that the empirical risks of source domains also need to be minimized. Such insights are well reflected in PhASER.

Theorem 2.6 (Non-stationarity Change of Hilbert Transform). *Suppose there are $M_{\mathcal{D}}$ samples (observations) available for a nonstationary time-series domain \mathcal{D}_x , and each sample $\mathbf{x}_i = \{x_{i,0}, \dots, x_{i,t}, \dots\}$ is characterized by its deterministic function, i.e., $\mathbf{x}_i(t) = x_{i,t} = x_i(t)$, $i \in [1, M_{\mathcal{D}}]$. If we apply Hilbert Transformation $\text{HT}(\mathbf{x}(t)) = \hat{\mathbf{x}}(t) = \int_{-\infty}^{\infty} \mathbf{x}(\tau) \frac{1}{\pi(t-\tau)} d\tau$ to augment these time-series samples, the nonstationary statistics of augmented samples are different from the original ones,*

$$\Pr_{\mathbf{x} \sim \hat{\mathcal{D}}_x}(\mathbf{x})(t) \neq \Pr_{\mathbf{x} \sim \mathcal{D}_x}(\mathbf{x})(t). \quad (15)$$

Insights. This theorem illustrates that Hilbert Transformation does change the nonstationary statistics of time series, providing theoretical support for proving our phase augmentation can diversify the non-stationarity of time series.

3. Experiments

We extensively evaluate the proposed PhASER framework against 10 state-of-the-art approaches on 5 datasets across three time-series applications. Our evaluation metric is per-segment accuracy. More implementation-specific details are given in Section D of Appendix. Our source codes are provided in the supplementary materials.

Datasets. We carry out experiments on three commonly used time-series applications – Human Activity Recognition (HAR), Sleep-Stage Classification (SSC), and Gesture Recognition (GR). For HAR, we use three benchmark datasets: 1) **WISDM** (Kwapisz et al., 2011) collected from 36 different users with 3 univariate dimensions, 2) **UCI-HAR** (Bulbul et al., 2018) collected from 30 people with 9 variates, and 3) **HHAR** (Stisen et al., 2015) collected

from 9 users with 3 feature dimensions. All HAR datasets consist of 6 distinct activities and their sequence length is 128. SSC (Goldberger et al., 2000) is built on continuously recorded single channel **EEG** from 20 healthy individuals segmented to a sequence length of 3000. As for GR (Lobov et al., 2018), we utilize 8-channel **EMG** signals to classify 6 different gestures with a sequence length of 200 and follow preprocessing steps similar to Lu et al. (2022b). And we follow the setup of ADATime (Ragab et al., 2023a) for HAR and SSC. More data-specific details are provided in Table 8 of Appendix.

Experimental Setup. Each dataset is partitioned into four diverse non-overlapping cross-domain scenarios, similar to Lu et al. (2023) and their detailed specification is provided in Section 8 of Appendix. 20% of the training data is kept aside as a validation set. The mean of three trials for each experiment is reported in the main text, and complete statistics are given in Section E of Appendix. Detailed experiment settings and hyperparameter choices are provided in Section D of Appendix.

Comparison Baselines. We conduct a comprehensive analysis with state-of-the-art approaches including standard domain generalization algorithms – ERM, DANN (Ganin et al., 2016), GroupDRO (Sagawa et al., 2019), RSC (Huang et al., 2020) and ANDMask (Parascandolo et al., 2020) implemented based on DomainBed benchmarking suite (Gulrajani & Lopez-Paz, 2020); audio domain generalization, BCResNet (Kim et al., 2021b); time-series representation learning, MAPU (Ragab et al., 2023b); and time-series domain generalizable learning, Diversify (Lu et al., 2022b). We also adapt a short-term time series forecasting model, Nonstationary Transformer (NSTrans) (Liu et al., 2022b), as a baseline along with another network-agnostic statistical technique, RevIN (Kim et al., 2021c) denoted as (Ours+RevIN*). We follow the default setups of these works and only conduct reasonable modifications for customizing them in our settings. More details are provided in Section D.2 of Appendix.

3.1. Effectiveness of PhASER across Applications

Human Activity Recognition. We view each person as a single domain and evaluate the generalization ability of PhASER framework under two settings, 1) *cross-person generalization*, where N_S ($N_S > 1$) source domains are used for training and the model is evaluated on unseen target domains, and 2) a more challenging scenario of *one-person-to-another*, where model is trained on one person ($N_S = 1$) and evaluated on another person. For the cross-person setting, we observe from Table 2 that the state-of-the-art domain generalization methods which are popular in vision-based domains do not perform equally well on time-series classification. This observation is consistent with previous works (Gagnon-Audet et al., 2022; Lu et al., 2022b) investigating out-of-domain generalization for time

Table 2. Classification accuracy of Target 1~4 scenarios for cross-person generalization in Human Activity Recognition on WISDM, HHAR, and UCIHAR datasets. The **best** and second-best results are bolded and underlined, respectively.

Dataset	WISDM					HHAR					UCIHAR					HAR
	1	2	3	4	Avg.	1	2	3	4	Avg.	1	2	3	4	Avg.	
ERM	0.57	0.50	0.51	0.55	0.53	0.49	0.46	0.45	0.47	0.47	0.72	0.64	0.70	0.72	0.70	0.57
GroupDRO	0.71	0.67	0.60	0.67	0.66	0.60	0.53	0.59	0.64	0.59	<u>0.91</u>	<u>0.84</u>	0.89	0.85	0.87	0.71
DANN	0.71	0.65	0.65	0.70	0.68	0.66	0.71	0.67	0.69	0.68	<u>0.84</u>	<u>0.79</u>	0.81	0.86	0.83	0.73
RSC	0.69	0.71	0.64	0.61	0.66	0.52	0.49	0.44	0.47	0.48	0.82	0.73	0.74	0.81	0.78	0.64
ANDMask	0.74	0.73	0.69	0.69	0.71	0.63	0.64	0.66	0.69	0.66	0.86	0.80	0.76	0.78	0.80	0.72
BCResNet	<u>0.83</u>	0.79	0.75	0.78	0.79	0.66	0.70	0.75	0.68	0.70	0.81	0.77	0.78	0.83	0.80	0.76
NSTrans	0.43	0.40	0.37	0.37	0.40	0.21	0.22	0.27	0.28	0.24	0.35	0.35	0.51	0.47	0.42	0.35
MAPU	0.75	0.69	0.79	0.79	0.75	0.73	0.72	0.81	<u>0.78</u>	0.76	0.85	0.80	0.85	0.82	0.83	0.78
Diversify	0.82	<u>0.82</u>	<u>0.84</u>	<u>0.81</u>	<u>0.82</u>	<u>0.82</u>	<u>0.76</u>	<u>0.82</u>	<u>0.68</u>	<u>0.77</u>	0.89	<u>0.84</u>	<u>0.93</u>	<u>0.90</u>	<u>0.89</u>	<u>0.83</u>
Ours+RevIN*	0.86	0.85	0.84	0.84	0.85	0.82	0.82	0.92	0.85	0.85	0.96	0.90	0.93	0.97	0.94	0.88
Ours	0.86	0.85	0.85	0.82	0.85	0.83	0.83	0.94	0.88	0.87	0.96	0.91	0.95	0.97	0.95	0.89

Table 3. Classification accuracy with Source 0~8 person for one-person-to-another generalization on HHAR dataset, with **best** and second-best results highlighted.

Source	0	1	2	3	4	5	6	7	8	Avg.
ERM	0.27	0.40	0.41	0.44	0.42	0.44	0.45	0.44	0.48	0.42
GroupDRO	0.33	0.53	0.38	0.48	0.47	0.51	0.47	0.48	0.49	0.46
DANN	0.32	0.44	0.42	0.45	0.42	0.48	0.49	0.45	0.51	0.44
RSC	0.27	0.45	<u>0.38</u>	0.45	0.40	0.47	0.50	0.44	0.53	0.43
ANDMask	0.34	0.50	0.37	0.43	0.46	0.51	0.46	0.47	0.52	0.45
BCResNet	0.28	0.48	0.32	0.47	0.42	0.52	0.44	0.45	0.49	0.43
NSTrans	0.20	0.22	0.17	0.20	0.21	0.22	0.26	0.17	0.20	0.21
MAPU	0.39	0.57	0.35	0.52	0.49	0.54	0.49	0.50	0.52	0.49
Diversify	0.42	0.62	0.32	<u>0.62</u>	<u>0.56</u>	<u>0.61</u>	<u>0.53</u>	<u>0.52</u>	<u>0.61</u>	<u>0.53</u>
Ours	0.53	0.70	0.63	0.66	0.64	0.67	0.65	0.67	0.62	0.64

series. **PhASER achieves the best out-of-domain generalization performance across all cases**, in particular, substantially outperforms the best baseline (Diversify) on WISDM, HHAR, and UCIHAR by 3%, 13%, and 6% respectively. For the more challenging one-person-to-another setting, we choose to test on HHAR dataset given its high non-stationarity among the three datasets (refer to Table 8 in Appendix for ADF stat). Table 3 reports the average accuracy when a model is trained on one person and evaluated on the remaining 8 people. **PhASER performs the best in such a setting as well**, outperforming the next best approach, Diversify, by almost 20%. These results strongly support the generalization performance of PhASER.

Sleep-Stage Classification. Next, we evaluate PhASER to classify five different sleep stages using EEG recordings in an attempt to conduct *cross-person generalization*. Past methods (Ragab et al., 2023a; He et al., 2023b) generally report the lowest performance in their respective settings for SSC tasks indicating its inherent complexity. The results in Table 4 (left) show that **PhASER provides the best performance in all cases** and achieves an average classification accuracy of 0.82 without accessing the domain labels or any target samples. It outperforms the best baseline (BCResNet) by 2% and the time-series domain generalization baseline

(Diversify) by almost 11%. The best performance of our method in this case highlights the value even in spectral representation of physiological time-series data.

Table 4. Classification accuracy for Target 1~4 scenarios for cross-person generalization in generalization Sleep-Stage Classification and Gesture Recognition using EEG and EMG, with **best** and second-best results highlighted.

Application	Sleep-Stage Classification					Gesture Recognition				
	1	2	3	4	Avg.	1	2	3	4	Avg.
ERM	0.50	0.46	0.49	0.45	0.47	0.45	0.58	0.57	0.54	0.54
GroupDRO	0.57	0.56	0.55	0.59	0.57	0.53	0.36	0.59	0.45	0.48
DANN	0.64	0.63	0.69	0.63	0.65	0.60	0.66	0.65	0.64	0.64
RSC	0.50	0.48	0.52	0.46	0.49	0.50	0.66	0.64	0.56	0.59
ANDMask	0.55	0.50	0.54	0.57	0.54	0.41	0.54	0.45	0.39	0.45
BCResNet	0.79	0.82	0.79	0.81	0.80	0.62	0.67	0.65	0.61	0.64
NSTrans	0.43	0.37	0.42	0.35	0.39	0.31	0.34	0.34	0.32	0.33
MAPU	0.69	0.68	0.65	0.69	0.68	0.64	0.69	0.71	0.68	0.68
Diversify	0.73	0.76	0.68	0.77	0.73	<u>0.68</u>	<u>0.80</u>	<u>0.75</u>	0.76	<u>0.75</u>
Ours	0.85	0.80	0.79	0.83	0.82	0.70	0.82	0.77	<u>0.75</u>	0.76

Gesture Recognition. In GR, the used bio-electronic signals are heavily influenced by user behavior and sensor time-varying properties, which correspond to natural non-stationarity. We follow Lu et al. (2023) to use 6 common classes when conducting our evaluations in a *cross-person setting*. The results in Table 4 (right) show that **PhASER offers the best performance in all cases except one**.

3.2. Ablation Study

We use two cases, HAR using WISDM and GR, to study the impact of each of our proposed design components as shown in Table 5. The first row indicates the performance of the complete PhASER framework and the following rows present the performance of different versions of PhASER with certain components detached or modified (details of how we detach or modify PhASER are provided in Section D of Appendix). From this table, we can observe that when the phase augmentation is not carried out (row 2), the performance significantly drops (by 11.6% on WISDM, and

5.8% on GR). Recall from our motivation study (refer to Table 1) that providing only magnitude as the input was the second best option compared to separate encoding. The results in rows 5 and 6 further support this observation, highlighting the importance of incorporating phase information for learning generalizable representations. Overall, we can observe that when ablating the phase-based residual and separate encoding structure (rows 3-7) the average performance drops by 10.6% and 13.7%, respectively. **This study demonstrates the value of all the components in PhASER.**

Table 5. Ablation analysis of PhASER on WISDM (a HAR dataset) and Gesture Recognition application. The inclusion of a component is denoted as \checkmark and exclusion as \times (modification).

	Phase Augmentation	Separate Encoders	F_{Pha} Residual	Accuracy	
				WISDM	GR
1	\checkmark	\checkmark	\checkmark	0.86	0.69
2	\times	\checkmark	\checkmark	0.81	0.61
3	\checkmark	\checkmark	$\times(F_{\text{Mag}} \text{ Res.})$	0.82	0.55
4	\checkmark	\checkmark	$\times(F_{\text{Fus}} \text{ Res.})$	0.84	0.60
5	\checkmark	\checkmark	\times	0.82	0.65
6	\checkmark	$\times(\text{Mag Only})$	\times	0.73	0.59
7	\checkmark	$\times(\text{Mag Only})$	$\times(F_{\text{Mag}} \text{ Res.})$	0.83	0.66

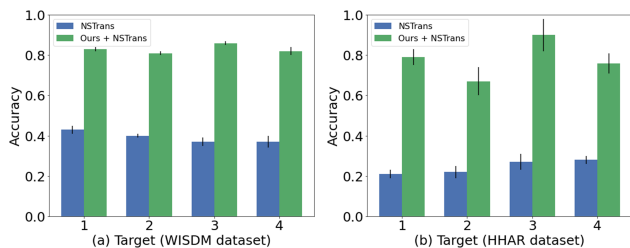


Figure 4. Illustration of significant improvement in average cross-person generalization performance of Nonstationary Transformer (NSTrans) from in (a) WISDM dataset from 0.40 to 0.83 and (b) HHAR dataset from 0.25 to 0.78, with our phase-driven approach.

3.3. General Applicability of PhASER

In addition to seamlessly incorporating plug-and-play modules like RevIN (Tables 2 and Tables 13, 14 in Appendix), we further demonstrate the general applicability and flexibility of PhASER by integrating the proposed three design elements into the NSTrans model: phase-based augmentation for diversifying non-stationarity, separate magnitude-phase feature encoding, and incorporation of the phase with a residual connection. The significant performance improvements on WISDM and HHAR (shown in Figure 4) demonstrate the general effectiveness of these proposed designs and the flexibility of PhASER with different backbone models. More details can be found in Section D.5 of Appendix.

4. Additional Related Works

Nonstationary Time-Series Analysis. In real-world scenarios, time series data are often nonstationary, posing significant challenges for forecasting and classification tasks (Es-

ling & Agon, 2012; Ismail Fawaz et al., 2019; Dama & Sinoquet, 2021; Wang et al., 2024). Solutions spanning from Bayesian models (Liang, 2005; Chen & Sun, 2021) and normalization techniques (Liu et al., 2023; Chang et al., 2021; Passalis et al., 2019) to recurrent neural networks (Tang et al., 2021; Du et al., 2021) and transformers (Liu et al., 2022c; Wang et al., 2022a) along with a few theoretical works for forecasting (Dama & Sinoquet, 2021) exist; there is a notable scarcity in theoretical works that analyze the challenges introduced by non-stationarity for time series classification. Although some studies (Zhao et al., 2020; Tonekaboni et al., 2020; Eldele et al., 2023) empirically validate the gains obtained by addressing non-stationarity, our work is the first to rigorously prove the crucial impact of non-stationarity on the time-series out-of-distribution classification.

Domain Generalizable Learning. While domain generalizable learning methods are well-established in visual data (Wang et al., 2022b), extending such capabilities to time-series data poses unique challenges. Traditional approaches like data augmentation (Wang et al., 2021b; Liu et al., 2022a; Wang et al., 2021a) and domain discrepancy minimization (Zhang & Chen, 2023; Li et al., 2018; Xu et al., 2021b) face limitations due to the less flexible nature of time-series augmentation and the broader concept of domains in this context (Wen et al., 2021; Wilson et al., 2020). Despite difficulties in domain discrepancy minimization for time series, some studies explore domain-invariant representation learning (Lu et al., 2023; Wang et al., 2023) and learnable data transformation (Qin et al., 2023; Mohapatra et al., 2023a; 2022). Different from these works, we emphasize the non-stationarity of time series and theoretically characterize it in the domain discrepancy. Some works in the visual domain have evidenced the role of phase in reducing domain discrepancy (Kim et al., 2023; Xu et al., 2021a) but they require sophisticated sampling strategy and domain labels. A handful of works (Lu et al., 2022a) in time-series applications hint at the role of phase for domain-invariant learning. Traditionally, signal-processing methods dictate sufficiency in phase-only information to reconstruct a signal (Masuyama et al., 2023; Jacques & Feuillen, 2020; 2021) under certain assumptions. Inspired by these, we propose a novel phase-driven framework including an augmentation module that can reasonably diversify the training data distribution and a representation learning mechanism that can deal with non-stationarity to minimize the domain discrepancy.

5. Conclusion

We address the generalization problem for nonstationary time-series classification using a phase-driven approach without accessing domain labels of source domains or samples from unseen distributions. Our approach consists of

phase-based phase augmentation, treating time-varying magnitude and phase as separate modalities and incorporating a novel phase-derived residual connection in the network. We support our design choices with rigorous theoretical and empirical evidence. Our method demonstrates significant improvement across 10 benchmarks on 5 real-world datasets, and our principles can be generally adapted to other works.

Impact Statement

PhASER, with its advanced approach to time-series domain-generalizable learning, offers significant societal benefits to various fields and domains, such as healthcare, financial, and manufacturing domains, by enabling more precise and dependable data analysis. While PhASER itself does not directly cause negative social impacts, its application within these critical areas necessitates a thoughtful examination of ethical concerns. In healthcare, PhASER can revolutionize patient monitoring and treatment, leading to improved experience and outcomes. In finance, it can enhance the stability and efficiency of financial markets. In manufacturing, we believe PhASER may help optimize production processes, reduce waste, and improve safety. However, the implementation of PhASER in such vital areas brings to the forefront ethical considerations like data privacy, bias prevention, and the careful management of automation reliance. Addressing these issues is important to leverage PhASER's benefits across these domains while ensuring ethical integrity and maintaining public trust in these areas.

References

- Bai, G., Ling, C., and Zhao, L. Temporal domain generalization with drift-aware dynamic neural networks. *arXiv preprint arXiv:2205.10664*, 2022.
- Bangaru, S. S., Wang, C., and Aghazadeh, F. Data quality and reliability assessment of wearable emg and imu sensor for construction activity recognition. *Sensors*, 20(18): 5264, 2020.
- Bulbul, E., Cetin, A., and Dogru, I. A. Human activity recognition using smartphones. In *2018 2nd international symposium on multidisciplinary studies and innovative technologies (ismsit)*, pp. 1–6. IEEE, 2018.
- Chang, S., Park, H., Cho, J., Park, H., Yun, S., and Hwang, K. Subspectral normalization for neural audio data processing. In *ICASSP 2021-2021 IEEE International Conference on Acoustics, Speech and Signal Processing (ICASSP)*, pp. 850–854. IEEE, 2021.
- Chen, X. and Sun, L. Bayesian temporal factorization for multidimensional time series prediction. *IEEE Transactions on Pattern Analysis and Machine Intelligence*, 44(9):4659–4673, 2021.
- Dama, F. and Sinoquet, C. Time series analysis and modeling to forecast: A survey. *arXiv preprint arXiv:2104.00164*, 2021.
- Du, Y., Wang, J., Feng, W., Pan, S., Qin, T., Xu, R., and Wang, C. Adarnn: Adaptive learning and forecasting of time series. In *Proceedings of the 30th ACM international conference on information & knowledge management*, pp. 402–411, 2021.
- Eldele, E., Ragab, M., Chen, Z., Wu, M., Kwoh, C.-K., Li, X., and Guan, C. Self-supervised contrastive representation learning for semi-supervised time-series classification. *IEEE Transactions on Pattern Analysis and Machine Intelligence*, 2023.
- Elfving, S., Uchibe, E., and Doya, K. Sigmoid-weighted linear units for neural network function approximation in reinforcement learning. *Neural networks*, 107:3–11, 2018.
- Esling, P. and Agon, C. Time-series data mining. *ACM Computing Surveys (CSUR)*, 45(1):1–34, 2012.
- Gagnon-Audet, J.-C., Ahuja, K., Darvishi-Bayazi, M.-J., Mousavi, P., Dumas, G., and Rish, I. Woods: Benchmarks for out-of-distribution generalization in time series. *arXiv preprint arXiv:2203.09978*, 2022.
- Ganin, Y., Ustinova, E., Ajakan, H., Germain, P., Larochelle, H., Laviolette, F., March, M., and Lempitsky, V. Domain-adversarial training of neural networks. *Journal of machine learning research*, 17(59):1–35, 2016.
- Germain, P., Habrard, A., Laviolette, F., and Morvant, E. A new pac-bayesian perspective on domain adaptation. In *International conference on machine learning*, pp. 859–868. PMLR, 2016.
- Goldberger, A. L., Amaral, L. A., Glass, L., Hausdorff, J. M., Ivanov, P. C., Mark, R. G., Mietus, J. E., Moody, G. B., Peng, C.-K., and Stanley, H. E. Physiobank, physiotoolkit, and physionet: components of a new research resource for complex physiologic signals. *circulation*, 101(23): e215–e220, 2000.
- Gulrajani, I. and Lopez-Paz, D. In search of lost domain generalization. *arXiv preprint arXiv:2007.01434*, 2020.
- Hayes, M., Lim, J., and Oppenheim, A. Signal reconstruction from phase or magnitude. *IEEE Transactions on Acoustics, Speech, and Signal Processing*, 28(6):672–680, 1980.
- He, F., Liu, T., and Tao, D. Why resnet works? residuals generalize. *IEEE transactions on neural networks and learning systems*, 31(12):5349–5362, 2020.

- He, H., Queen, O., Koker, T., Cuevas, C., Tsiligkaridis, T., and Zitnik, M. Domain adaptation for time series under feature and label shifts. *arXiv preprint arXiv:2302.03133*, 2023a.
- He, H., Queen, O., Koker, T., Cuevas, C., Tsiligkaridis, T., and Zitnik, M. Domain adaptation for time series under feature and label shifts. *arXiv preprint arXiv:2302.03133*, 2023b.
- He, K., Zhang, X., Ren, S., and Sun, J. Deep residual learning for image recognition. In *Proceedings of the IEEE conference on computer vision and pattern recognition*, pp. 770–778, 2016.
- Huang, N. E. *Hilbert-Huang transform and its applications*, volume 16. World Scientific, 2014.
- Huang, Z., Wang, H., Xing, E. P., and Huang, D. Self-challenging improves cross-domain generalization. In *Computer Vision–ECCV 2020: 16th European Conference, Glasgow, UK, August 23–28, 2020, Proceedings, Part II 16*, pp. 124–140. Springer, 2020.
- Ismail Fawaz, H., Forestier, G., Weber, J., Idoumghar, L., and Muller, P.-A. Deep learning for time series classification: a review. *Data mining and knowledge discovery*, 33(4):917–963, 2019.
- Iwana, B. K. and Uchida, S. An empirical survey of data augmentation for time series classification with neural networks. *Plos one*, 16(7):e0254841, 2021.
- Jacques, L. and Feuille, T. Keep the phase! signal recovery in phase-only compressive sensing. *arXiv preprint arXiv:2011.06499*, 2020.
- Jacques, L. and Feuille, T. The importance of phase in complex compressive sensing. *IEEE Transactions on Information Theory*, 67(6):4150–4161, 2021.
- Kazemi, S. M., Goel, R., Eghbali, S., Ramanan, J., Sahota, J., Thakur, S., Wu, S., Smyth, C., Poupart, P., and Brubaker, M. Time2vec: Learning a vector representation of time. *arXiv preprint arXiv:1907.05321*, 2019.
- Kemp, B., Zwinderman, A. H., Tuk, B., Kamphuisen, H. A., and Obery, J. J. Analysis of a sleep-dependent neuronal feedback loop: the slow-wave microcontinuity of the eeg. *IEEE Transactions on Biomedical Engineering*, 47(9):1185–1194, 2000.
- Kim, B., Chang, S., Lee, J., and Sung, D. Broadcasted residual learning for efficient keyword spotting. *arXiv preprint arXiv:2106.04140*, 2021a.
- Kim, B., Yang, S., Kim, J., and Chang, S. Domain generalization on efficient acoustic scene classification using residual normalization. *arXiv preprint arXiv:2111.06531*, 2021b.
- Kim, M., Li, D., and Hospedales, T. Domain generalisation via domain adaptation: An adversarial fourier amplitude approach. *arXiv preprint arXiv:2302.12047*, 2023.
- Kim, T., Kim, J., Tae, Y., Park, C., Choi, J.-H., and Choo, J. Reversible instance normalization for accurate time-series forecasting against distribution shift. In *International Conference on Learning Representations*, 2021c.
- King, F. W. *Hilbert Transforms: Volume 2*, volume 2. Cambridge University Press, 2009.
- Kingma, D. P., Ba, J. A., and Adam, J. A method for stochastic optimization. arxiv 2014. *arXiv preprint arXiv:1412.6980*, 106, 2020.
- Kwapisz, J. R., Weiss, G. M., and Moore, S. A. Activity recognition using cell phone accelerometers. *ACM SigKDD Explorations Newsletter*, 12(2):74–82, 2011.
- Lang, S. and Lang, S. The plancherel formula. *SL 2 (R)*, pp. 163–177, 1985.
- Li, H., Pan, S. J., Wang, S., and Kot, A. C. Domain generalization with adversarial feature learning. In *Proceedings of the IEEE conference on computer vision and pattern recognition*, pp. 5400–5409, 2018.
- Li, J., Sun, A., Han, J., and Li, C. A survey on deep learning for named entity recognition. *IEEE Transactions on Knowledge and Data Engineering*, 34(1):50–70, 2020.
- Li, P., Li, D., Li, W., Gong, S., Fu, Y., and Hospedales, T. M. A simple feature augmentation for domain generalization. In *Proceedings of the IEEE/CVF International Conference on Computer Vision*, pp. 8886–8895, 2021.
- Liang, F. Bayesian neural networks for nonlinear time series forecasting. *Statistics and computing*, 15:13–29, 2005.
- Liu, C., Wang, L., Lyu, L., Sun, C., Wang, X., and Zhu, Q. Deja vu: Continual model generalization for unseen domains. In *The Eleventh International Conference on Learning Representations*, 2022a.
- Liu, Y., Wu, H., Wang, J., and Long, M. Non-stationary transformers: Rethinking the stationarity in time series forecasting. *arXiv preprint arXiv:2205.14415*, 2022b.
- Liu, Y., Wu, H., Wang, J., and Long, M. Non-stationary transformers: Exploring the stationarity in time series forecasting. *Advances in Neural Information Processing Systems*, 35:9881–9893, 2022c.

- Liu, Z., Cheng, M., Li, Z., Huang, Z., Liu, Q., Xie, Y., and Chen, E. Adaptive normalization for non-stationary time series forecasting: A temporal slice perspective. In *Thirty-seventh Conference on Neural Information Processing Systems*, 2023.
- Lobov, S., Krilova, N., Kastalskiy, I., Kazantsev, V., and Makarov, V. A. Latent factors limiting the performance of semg-interfaces. *Sensors*, 18(4):1122, 2018.
- Lu, W., Wang, J., Li, H., Chen, Y., and Xie, X. Domain-invariant feature exploration for domain generalization. *arXiv preprint arXiv:2207.12020*, 2022a.
- Lu, W., Wang, J., Sun, X., Chen, Y., and Xie, X. Out-of-distribution representation learning for time series classification. In *The Eleventh International Conference on Learning Representations*, 2022b.
- Lu, W., Wang, J., Sun, X., Chen, Y., and Xie, X. Out-of-distribution representation learning for time series classification. In *The Eleventh International Conference on Learning Representations*, 2023. URL <https://openreview.net/forum?id=gUZWOE4216Q>.
- Marion, P., Wu, Y.-H., Sander, M. E., and Biau, G. Implicit regularization of deep residual networks towards neural odes. *arXiv preprint arXiv:2309.01213*, 2023.
- Masuyama, Y., Ueno, N., and Ono, N. Signal reconstruction from mel-spectrogram based on bi-level consistency of full-band magnitude and phase. In *2023 IEEE Workshop on Applications of Signal Processing to Audio and Acoustics (WASPAA)*, pp. 1–5. IEEE, 2023.
- Mohapatra, P., Pandey, A., Islam, B., and Zhu, Q. Speech disfluency detection with contextual representation and data distillation. In *Proceedings of the 1st ACM International Workshop on Intelligent Acoustic Systems and Applications*, pp. 19–24, 2022.
- Mohapatra, P., Islam, B., Islam, M. T., Jiao, R., and Zhu, Q. Efficient stuttering event detection using siamese networks. In *ICASSP 2023-2023 IEEE International Conference on Acoustics, Speech and Signal Processing (ICASSP)*, pp. 1–5. IEEE, 2023a.
- Mohapatra, P., Pandey, A., Keten, S., Chen, W., and Zhu, Q. Person identification with wearable sensing using missing feature encoding and multi-stage modality fusion. In *ICASSP 2023-2023 IEEE International Conference on Acoustics, Speech and Signal Processing (ICASSP)*, pp. 1–2. IEEE, 2023b.
- Mohapatra, P., Pandey, A., Sui, Y., and Zhu, Q. Effect of attention and self-supervised speech embeddings on non-semantic speech tasks. In *Proceedings of the 31st ACM International Conference on Multimedia*, pp. 9511–9515, 2023c.
- Ozdemir, M. A., Kisa, D. H., Guren, O., Onan, A., and Akan, A. Emg based hand gesture recognition using deep learning. In *2020 Medical Technologies Congress (TIPTEKNO)*, pp. 1–4. IEEE, 2020.
- Parascandolo, G., Neitz, A., Orvieto, A., Gresele, L., and Schölkopf, B. Learning explanations that are hard to vary. *arXiv preprint arXiv:2009.00329*, 2020.
- Passalis, N., Tefas, A., Kannianen, J., Gabbouj, M., and Iosifidis, A. Deep adaptive input normalization for time series forecasting. *IEEE transactions on neural networks and learning systems*, 31(9):3760–3765, 2019.
- Phaye, S. S. R., Benetos, E., and Wang, Y. Subspectralnet—using sub-spectrogram based convolutional neural networks for acoustic scene classification. In *ICASSP 2019-2019 IEEE International Conference on Acoustics, Speech and Signal Processing (ICASSP)*, pp. 825–829. IEEE, 2019.
- Qin, X., Wang, J., Ma, S., Lu, W., Zhu, Y., Xie, X., and Chen, Y. Generalizable low-resource activity recognition with diverse and discriminative representation learning. *KDD*, 2023.
- Ragab, M., Eldele, E., Tan, W. L., Foo, C.-S., Chen, Z., Wu, M., Kwok, C.-K., and Li, X. Adatime: A benchmarking suite for domain adaptation on time series data. *ACM Transactions on Knowledge Discovery from Data*, 17(8): 1–18, 2023a.
- Ragab, M., Eldele, E., Wu, M., Foo, C.-S., Li, X., and Chen, Z. Source-free domain adaptation with temporal imputation for time series data. In *Proceedings of the 29th ACM SIGKDD Conference on Knowledge Discovery and Data Mining*, pp. 1989–1998, 2023b.
- Sagawa, S., Koh, P. W., Hashimoto, T. B., and Liang, P. Distributionally robust neural networks for group shifts: On the importance of regularization for worst-case generalization. *arXiv preprint arXiv:1911.08731*, 2019.
- Said, S. E. and Dickey, D. A. Testing for unit roots in autoregressive-moving average models of unknown order. *Biometrika*, 71(3):599–607, 1984.
- Stisen, A., Blunck, H., Bhattacharya, S., Prentow, T. S., Kjærgaard, M. B., Dey, A., Sonne, T., and Jensen, M. M. Smart devices are different: Assessing and mitigating mobile sensing heterogeneities for activity recognition. In *Proceedings of the 13th ACM conference on embedded networked sensor systems*, pp. 127–140, 2015.
- Tang, X.-s., Hao, K., and Wei, H. A bio-inspired positional embedding network for transformer-based models. *Neural Networks*, 166:204–214, 2023.

- Tang, Y., Yu, F., Pedrycz, W., Yang, X., Wang, J., and Liu, S. Building trend fuzzy granulation-based lstm recurrent neural network for long-term time-series forecasting. *IEEE transactions on fuzzy systems*, 30(6):1599–1613, 2021.
- Tonekaboni, S., Eytan, D., and Goldenberg, A. Unsupervised representation learning for time series with temporal neighborhood coding. In *International Conference on Learning Representations*, 2020.
- Van Erven, T. and Harremoës, P. Rényi divergence and kullback-leibler divergence. *IEEE Transactions on Information Theory*, 60(7):3797–3820, 2014.
- Vaswani, A., Shazeer, N., Parmar, N., Uszkoreit, J., Jones, L., Gomez, A. N., Kaiser, Ł., and Polosukhin, I. Attention is all you need. *Advances in neural information processing systems*, 30, 2017.
- Virtanen, P., Gommers, R., Oliphant, T. E., Haberland, M., Reddy, T., Cournapeau, D., Burovski, E., Peterson, P., Weckesser, W., Bright, J., van der Walt, S. J., Brett, M., Wilson, J., Millman, K. J., Mayorov, N., Nelson, A. R. J., Jones, E., Kern, R., Larson, E., Carey, C. J., Polat, İ., Feng, Y., Moore, E. W., VanderPlas, J., Laxalde, D., Perktold, J., Cimrman, R., Henriksen, I., Quintero, E. A., Harris, C. R., Archibald, A. M., Ribeiro, A. H., Pedregosa, F., van Mulbregt, P., and SciPy 1.0 Contributors. SciPy 1.0: Fundamental Algorithms for Scientific Computing in Python. *Nature Methods*, 17:261–272, 2020. doi: 10.1038/s41592-019-0686-2.
- Volpi, R., Namkoong, H., Sener, O., Duchi, J. C., Murino, V., and Savarese, S. Generalizing to unseen domains via adversarial data augmentation. *Advances in neural information processing systems*, 31, 2018.
- Wang, H., Wang, T., Li, S., Zheng, J., Guan, S., and Chen, W. Adaptive long-short pattern transformer for stock investment selection. In *Proceedings of the Thirty-First International Joint Conference on Artificial Intelligence*, pp. 3970–3977, 2022a.
- Wang, J., Lan, C., Liu, C., Ouyang, Y., Qin, T., Lu, W., Chen, Y., Zeng, W., and Yu, P. Generalizing to unseen domains: A survey on domain generalization. *IEEE Transactions on Knowledge and Data Engineering*, 2022b.
- Wang, J., Chen, L., and Al Faruque, M. A. Domino: Domain-invariant hyperdimensional classification for multi-sensor time series data. In *2023 IEEE/ACM International Conference on Computer Aided Design (ICCAD)*, pp. 1–9. IEEE, 2023.
- Wang, L., Xu, S., Xu, R., Wang, X., and Zhu, Q. Non-transferable learning: A new approach for model ownership verification and applicability authorization. In *International Conference on Learning Representations*, 2021a.
- Wang, L., Xu, S., Du, X., and Zhu, Q. Dacr: Distribution-augmented contrastive reconstruction for time-series anomaly detection. *arXiv preprint arXiv:2401.11271*, 2024.
- Wang, Z., Luo, Y., Qiu, R., Huang, Z., and Baktashmotlagh, M. Learning to diversify for single domain generalization. In *Proceedings of the IEEE/CVF International Conference on Computer Vision*, pp. 834–843, 2021b.
- Wen, Q., Sun, L., Yang, F., Song, X., Gao, J., Wang, X., and Xu, H. Time series data augmentation for deep learning: A survey. *arXiv preprint arXiv:2002.12478*, 2020.
- Wen, Q., Sun, L., Yang, F., Song, X., Gao, J., Wang, X., and Xu, H. Time series data augmentation for deep learning: A survey. In *Proceedings of the Thirtieth International Joint Conference on Artificial Intelligence*. International Joint Conferences on Artificial Intelligence Organization, 2021.
- Wilson, G., Doppa, J. R., and Cook, D. J. Multi-source deep domain adaptation with weak supervision for time-series sensor data. In *Proceedings of the 26th ACM SIGKDD international conference on knowledge discovery & data mining*, pp. 1768–1778, 2020.
- Xu, Q., Zhang, R., Zhang, Y., Wang, Y., and Tian, Q. A fourier-based framework for domain generalization. In *Proceedings of the IEEE/CVF Conference on Computer Vision and Pattern Recognition*, pp. 14383–14392, 2021a.
- Xu, S., Wang, L., Wang, Y., and Zhu, Q. Weak adaptation learning: Addressing cross-domain data insufficiency with weak annotator. In *Proceedings of the IEEE/CVF International Conference on Computer Vision*, pp. 8917–8926, 2021b.
- Xu, X., Zhang, H., Sefidgar, Y., Ren, Y., Liu, X., Seo, W., Brown, J., Kuehn, K., Merrill, M., Nurius, P., et al. Globem dataset: Multi-year datasets for longitudinal human behavior modeling generalization. *Advances in Neural Information Processing Systems*, 35:24655–24692, 2022.
- Yan, S., Liu, C., Yu, Z., Ju, L., Mahapatra, D., Betz-Stablein, B., Mar, V., Janda, M., Soyer, P., and Ge, Z. Prompt-driven latent domain generalization for medical image classification. *arXiv preprint arXiv:2401.03002*, 2024.
- Yang, L. and Hong, S. Unsupervised time-series representation learning with iterative bilinear temporal-spectral fusion. In *International Conference on Machine Learning*, pp. 25038–25054. PMLR, 2022.

Zhang, X. and Chen, Y.-C. Adaptive domain generalization via online disagreement minimization. *IEEE Transactions on Image Processing*, 2023.

Zhao, H., Zheng, Q., Ma, K., Li, H., and Zheng, Y. Deep representation-based domain adaptation for nonstationary eeg classification. *IEEE Transactions on Neural Networks and Learning Systems*, 32(2):535–545, 2020.

Appendix

This Appendix includes additional details for the paper “Phase-driven Domain Generalizable Learning for Nonstationary Time Series”, including the reproducibility statement, theoretical proofs (Section A), detailed dataset introduction (Section C), more details of PHASER (Section B), and implementation details (Section D) and detailed results (Section E) of main experiments.

Reproducibility Statement

All source codes to reproduce experiment results (with instructions for running the code) have been provided in the Supplementary Materials. We use public datasets and provide implementation details in the following sections.

A. Theoretical Proofs

Lemma 2.4. Let a set S of source domains $S = \{\mathcal{S}_i\}_{i=1}^{N_S}$. A convex hull Λ_S is considered here that consists of mixture distributions $\Lambda_S = \{\bar{\mathcal{S}} : \bar{\mathcal{S}}(\cdot) = \sum_{i=1}^{N_S} \pi_i \mathcal{S}_i(\cdot), \pi_i \in \Delta_{N_S-1}\}$, where Δ_{N_S-1} is the $N_S - 1$ -th dimensional simplex. Let $\beta_q(\mathcal{S}_i \| \mathcal{S}_j) \leq \epsilon$ for $\forall i, j \in [N_S]$, we have the following relation for the β -Divergence between any pair of two domains $\mathcal{D}', \mathcal{D}'' \in \Lambda_S$ in the convex hull,

$$\beta_q(\mathcal{D}' \| \mathcal{D}'') \leq \epsilon. \quad (16)$$

Proof. Suppose two unseen domains \mathcal{D}' and \mathcal{D}'' on the convex hull Λ_S of N_S source domains with support Ω . More specifically, let these two domains be $\mathcal{D}' = \sum_{k=1}^{N_S} \pi_k \mathcal{S}_k(\cdot)$ and $\mathcal{D}'' = \sum_{l=1}^{N_S} \pi_l \mathcal{S}_l(\cdot)$, then the β -Divergence between \mathcal{D}' and \mathcal{D}'' is

$$\beta_q(\mathcal{D}' \| \mathcal{D}'') = 2^{\frac{q-1}{q}} \text{RD}_q(\mathcal{D}' \| \mathcal{D}''). \quad (17)$$

Let us consider the part of Rényi Divergence as follows,

$$\begin{aligned} \text{RD}_q(\mathcal{D}' \| \mathcal{D}'') &= \frac{1}{q-1} \ln \int_{\Omega} [\mathcal{D}'(x)]^q [\mathcal{D}''(x)]^{1-q} dx \\ &= \frac{1}{q-1} \ln \int_{\Omega} \left[\sum_{k=1}^{N_S} \pi_k \mathcal{S}_k(x) \right]^q \left[\sum_{l=1}^{N_S} \pi_l \mathcal{S}_l(x) \right]^{1-q} dx \\ &= \frac{1}{q-1} \ln \int_{\Omega} \left[\sum_{k=1}^{N_S} \sum_{l=1}^{N_S} \pi_k \pi_l \mathcal{S}_k(x) \right]^q \left[\sum_{k=1}^{N_S} \sum_{l=1}^{N_S} \pi_k \pi_l \mathcal{S}_l(x) \right]^{1-q} dx \\ &= \frac{1}{q-1} \ln \sum_{k=1}^{N_S} \sum_{l=1}^{N_S} \pi_k \pi_l \int_{\Omega} [\mathcal{S}_k(x)]^q [\mathcal{S}_l(x)]^{1-q} dx \\ &\leq \frac{1}{q-1} \ln \sum_{k=1}^{N_S} \sum_{l=1}^{N_S} \pi_k \pi_l \max_{k, l \in [N_S]} \int_{\Omega} [\mathcal{S}_k(x)]^q [\mathcal{S}_l(x)]^{1-q} dx \\ &= \frac{1}{q-1} \ln \max_{k, l \in [N_S]} \int_{\Omega} [\mathcal{S}_k(x)]^q [\mathcal{S}_l(x)]^{1-q} dx. \end{aligned} \quad (18)$$

According to the given assumption that $\beta_q(\mathcal{S}_i \| \mathcal{S}_j) \leq \epsilon$ for $\forall i, j \in [N_S]$, we have,

$$\text{RD}_q(\mathcal{D}' \| \mathcal{D}'') \leq \frac{1}{q-1} \ln \max_{k, l \in [N_S]} \int_{\Omega} [\mathcal{S}_k(x)]^q [\mathcal{S}_l(x)]^{1-q} dx = \max_{k, l \in [N_S]} \text{RD}_q(\mathcal{S}_k \| \mathcal{S}_l) \leq \frac{q}{q-1} \log_2 \epsilon. \quad (19)$$

Thus $\beta_q(\mathcal{D}' \| \mathcal{D}'') \leq \epsilon$. \square

Theorem 2.5. Let \mathcal{H} be a hypothesis space built from a set of source time-series domains $S = \{\mathcal{S}_i\}_{i=1}^{N_S}$ with the same value range (i.e., the supports of these source domains are the same). Suppose $q > 0$ is a constant, for any unseen time-series

domain \mathcal{D}_U from the convex hull Λ_S , we have its closest element $\mathcal{D}_{\bar{U}}$ in Λ_S , i.e., $\mathcal{D}_{\bar{U}} = \arg \min_{\pi_1, \dots, \pi_{N_S}} \beta_q(\mathcal{D}_{\bar{U}} \| \sum_{i=1}^{N_S} \pi_i \mathcal{S}_i)$. Then the risk of \mathcal{D}_U on any ρ in \mathcal{H} is,

$$R_{\mathcal{D}_U}[\rho] \leq \frac{1}{2} d_{\mathcal{D}_U}(\rho) + \epsilon \cdot [e_{\mathcal{D}_{\bar{U}}}(\rho)]^{1-\frac{1}{q}}, \quad (20)$$

where $d_{\mathcal{D}}(\rho)$ and $e_{\mathcal{D}}(\rho)$ are an expected disagreement and an expected joint error of a domain \mathcal{D} , respectively, and they are defined as follows,

$$d_{\mathcal{D}}(\rho) = \mathbb{E}_{\mathbf{x} \sim \mathcal{D}_x} \mathbb{E}_{h \sim \rho} \mathbb{E}_{h' \sim \rho} \mathbb{I}[h(\mathbf{x}) \neq h'(\mathbf{x})], \quad (21)$$

$$e_{\mathcal{D}}(\rho) = \mathbb{E}_{(\mathbf{x}, y) \sim \mathcal{D}} \mathbb{E}_{h \sim \rho} \mathbb{E}_{h' \sim \rho} \mathbb{I}[h(\mathbf{x}) \neq y] \mathbb{I}[h'(\mathbf{x}) \neq y], \quad (22)$$

where $\mathbb{I}[\cdot]$ is an indicator function with $\mathbb{I}[\text{True}] = 1$ and $\mathbb{I}[\text{False}] = 0$. The ϵ in Eq. (12) is a value larger than the maximum β -Divergence in Λ_S ,

$$\epsilon \geq \max_{i, j \in [N_S], i \neq j, t \in [0, +\infty)} 2^{\frac{q-1}{q}} \text{RD}_q(\mathcal{S}_i(t) \| \mathcal{S}_j(t)), \quad (23)$$

where

$$\text{RD}_q(\mathcal{S}_i(t) \| \mathcal{S}_j(t)) = \frac{q(\mu_{j,t} - \mu_{i,t})^2}{2(1-q)\sigma_{i,t}^2 + 2\sigma_{j,t}^2} + \frac{\ln \frac{\sqrt{(1-q)\sigma_{i,t}^2 + \sigma_{j,t}^2}}{\sigma_{i,t}^{1-q} \sigma_{j,t}^q}}{1-q}}{1-q} \quad (24)$$

Proof. According to Theorem 3 of Germain et al. (2016), if \mathcal{H} is a hypothesis space, and \mathcal{S}, \mathcal{T} respectively are the source and target domains. For all ρ in \mathcal{H} ,

$$R_{\mathcal{T}}[\rho] \leq \frac{1}{2} d_{\mathcal{T}}(\rho) + \beta_q(\mathcal{T} \| \mathcal{S}) \cdot [e_{\mathcal{S}}(\rho)]^{1-\frac{1}{q}} + \eta_{\mathcal{T} \setminus \mathcal{S}}, \quad (25)$$

where $\eta_{\mathcal{T} \setminus \mathcal{S}}$ denotes the distribution of $(\mathbf{x}, y) \sim \mathcal{T}$ conditional to $(\mathbf{x}, y) \in \text{SUPP}(\mathcal{S})$. But because it is hardly conceivable to estimate the joint error $e_{\mathcal{T} \setminus \mathcal{S}}(\rho)$ without making extra assumptions, Germain et al. (2016) defines the worst risk for this unknown area,

$$\eta_{\mathcal{T} \setminus \mathcal{S}} = \Pr_{(\mathbf{x}, y) \sim \mathcal{T}} [(\mathbf{x}, y) \notin \text{SUPP}(\mathcal{S})] \sup_{h \in \mathcal{H}} R_{\mathcal{T} \setminus \mathcal{S}}[h]. \quad (26)$$

In Theorem 2.5, all domains from the convex hull Λ_S have the same value range, in other words, their supports are continuous and fully overlapped. In this case, $\Pr_{(\mathbf{x}, y) \sim \mathcal{T}} [(\mathbf{x}, y) \notin \text{SUPP}(\mathcal{S})] = 0$, i.e., $\eta_{\mathcal{T} \setminus \mathcal{S}} = 0$.

With Eq. (25), if the target domain \mathcal{T} is assumed as an unseen domain \mathcal{D}_U from the convex hull Λ_S , and we select its closest element $\mathcal{D}_{\bar{U}} = \arg \min_{\pi_1, \dots, \pi_{N_S}} \beta_q(\mathcal{D}_{\bar{U}} \| \sum_{i=1}^{N_S} \pi_i \mathcal{S}_i)$ and regard it as the source domain, we can derive Eq. (25) into

$$R_{\mathcal{D}_U}[\rho] \leq \frac{1}{2} d_{\mathcal{D}_U}(\rho) + \beta_q(\mathcal{D}_U \| \mathcal{D}_{\bar{U}}) \cdot [e_{\mathcal{D}_{\bar{U}}}(\rho)]^{1-\frac{1}{q}} + 0. \quad (27)$$

Then according to Lemma 2.4, as both \mathcal{D}_U and $\mathcal{D}_{\bar{U}}$ are from the convex hull Λ_S , $\beta_q(\mathcal{D}_U \| \mathcal{D}_{\bar{U}}) \leq \epsilon$. As for acquiring Eq. (14), we only need to substitute the time series domains in the form of random variable distributions into the Rényi Divergence. □

Theorem 2.6. Suppose there are $M_{\mathcal{D}}$ samples (observations) available for a non-stationary time-series domain \mathcal{D}_x , and each sample $\mathbf{x}_i = \{x_{i,0}, \dots, x_{i,t}, \dots\}$ is characterized by its deterministic function, i.e., $\mathbf{x}_i(t) = x_{i,t} = x_i(t)$, $i \in [1, M_{\mathcal{D}}]$. If we apply Hilbert Transformation $\text{HT}(\mathbf{x}(t)) = \hat{\mathbf{x}}(t) = \int_{-\infty}^{\infty} x(\tau) \frac{1}{\pi(t-\tau)} d\tau$ to augment these time-series samples, the non-stationary statistics of augmented samples are different from the original ones,

$$\Pr_{\mathbf{x} \sim \hat{\mathcal{D}}_x}(\mathbf{x})(t) \neq \Pr_{\mathbf{x} \sim \mathcal{D}_x}(\mathbf{x})(t). \quad (28)$$

Proof. According to Definition 2.1, the statistics of the non-stationary time-series domain consist of non-stationary mean and variance. To prove Theorem 2.6, we only need to prove that the mean of the time-series domain changes after applying Hilbert Transformation (HT). HT can only be conducted on deterministic signals, thus we use the empirical statistics of $M_{\mathcal{D}}$ samples to approximate the real statistics,

$$\mathbb{E}_{\mathbf{x} \sim \widehat{\mathcal{D}}_{\mathbf{x}}}(\mathbf{x})(t) = \sum_{i=1}^{M_{\mathcal{D}}} \widehat{\mathbf{x}}_i(t) = \widehat{\mu}_t, \quad \mathbb{E}_{\mathbf{x} \sim \mathcal{D}_{\mathbf{x}}}(\mathbf{x})(t) = \sum_{i=1}^{M_{\mathcal{D}}} \mathbf{x}_i(t) = \mu_t. \quad (29)$$

According to the standard definition of HT (King, 2009) and the linear property of integral operation, we have

$$\mathbb{E}_{\mathbf{x} \sim \widehat{\mathcal{D}}_{\mathbf{x}}}(\mathbf{x})(t) = \sum_{i=1}^{M_{\mathcal{D}}} \widehat{\mathbf{x}}_i(t) = \sum_{i=1}^{M_{\mathcal{D}}} \int_{-\infty}^{\infty} \mathbf{x}_i(\tau) \frac{1}{\pi(t-\tau)} d\tau = \int_{-\infty}^{\infty} \sum_{i=1}^{M_{\mathcal{D}}} \left[\mathbf{x}_i(\tau) \frac{1}{\pi(t-\tau)} d\tau \right] = \frac{1}{\pi} \int_{-\infty}^{\infty} \frac{\mu_{\tau}}{t-\tau} d\tau. \quad (30)$$

To interpret Eq. (30), we can assume there is a new signal $\mathbf{s} = \{\mu_0, \dots, \mu_t, \dots\}$ with the deterministic function $\mu_t = u(t)$, and we next apply proof by contradiction for the following proof. Suppose the non-stationary statistics of the original and HT-transformed samples are identical, i.e., $\mathbb{E}_{\mathbf{x} \sim \widehat{\mathcal{D}}_{\mathbf{x}}}(\mathbf{x})(t) = \mathbb{E}_{\mathbf{x} \sim \mathcal{D}_{\mathbf{x}}}(\mathbf{x})(t)$, we can derive the following formula,

$$\frac{1}{\pi} \int_{-\infty}^{\infty} \frac{u(\tau)}{t-\tau} d\tau = u(t), \quad (31)$$

which indicates that the HT-transformed $\widehat{\mathbf{s}}$ is identical to the original \mathbf{s} . HT has a property called Orthogonality (King, 2009): if $\mathbf{x}(t)$ is a real-valued energy signal, then $\mathbf{x}(t)$ and its HT-transformed signal $\widehat{\mathbf{x}}(t)$ are orthogonal, i.e.,

$$\int_{-\infty}^{\infty} \mathbf{x}(t) \widehat{\mathbf{x}}(t) dt = 0. \quad (32)$$

To prove the property of Orthogonality, we need to use Plancherel's Formula,

Theorem A.1 (Plancherel's Formula (Lang & Lang, 1985)). *Suppose that $u, v \in L^1(\mathbb{R}) \cap L^2(\mathbb{R})$, then*

$$\int_{-\infty}^{\infty} u(t) \overline{v(t)} dt = \frac{1}{2\pi} \int_{-\infty}^{\infty} \mathcal{F}u(\omega) \overline{\mathcal{F}v(\omega)} d\omega, \quad (33)$$

where $L^1(\cdot), L^2(\cdot)$ denote the L^p spaces with $p = 1, p = 2$ respectively, \mathbb{R} represents the real-valued space, and \mathcal{F} denotes the Plancherel transformation.

With Plancherel's Formula, we can prove the property of Orthogonality as follows,

$$\begin{aligned} \int_{-\infty}^{\infty} \mathbf{x}(t) \widehat{\mathbf{x}}(t) dt &= \frac{1}{2\pi} \int_{-\infty}^{\infty} \mathcal{F}(\omega) (-i \operatorname{sgn}(\omega) \mathcal{F}(\omega))^* d\omega \\ &= \frac{i}{2\pi} \int_{-\infty}^{\infty} \operatorname{sgn}(\omega) \mathcal{F}(\omega) \mathcal{F}^*(\omega) d\omega \\ &= \frac{i}{2\pi} \int_{-\infty}^{\infty} \operatorname{sgn}(\omega) |\mathcal{F}(\omega)|^2 d\omega \\ &= 0, \end{aligned} \quad (34)$$

where $\operatorname{sgn}(\cdot)$ is a sign function. After proving the Orthogonality, we can use it with the condition of Eq. (31), i.e.,

$$\int_{-\infty}^{\infty} u(t) \widehat{u}(t) dt = \int_{-\infty}^{\infty} u^2(t) dt = 0. \quad (35)$$

Eq. (35) holds true only if $\forall t \in [0, +\infty), u(t) = 0$, which is contradict to our initial assumption that $\mu_t = u(t)$ is not always zero in Definition 2.1. As a result, the assumption of $\widehat{\mu}_t = \mu_t$ is false. \square

B. Additional Details on PhASER

Augmented Dickey Fuller (ADF) Test. This is a statistical tool to assess the non-stationarity of a given time-series signal. This test operates under a null hypothesis \mathbb{H}_0 where the signal has a *unit-root*. The existence of *unit-root* is a guarantee that the signal is non-stationary (Said & Dickey, 1984). To reject \mathbb{H}_0 , the statistic value of the ADF test should be less than the critical values associated with a significance level of 0.05 (denoted by p , the probability of observing such a test statistic under the null hypothesis). Throughout the paper, for multivariate time series, the average ADF statistics across all variates are reported. Besides, since this is a statistical tool to evaluate non-stationarity for each instance of time-series data, we provide an average of this number across a dataset to give the reader a view of the degree of non-stationarity.

Phase Augmentation In this work, we are particularly interested in learning representations robust to temporal distribution shifts. Incorporating a phase shift in a signal is a less-studied augmentation technique. One of the main challenges is that real-world signals are not composed of a single frequency component and accurately estimating and controlling the shifting of the phase while retaining the magnitude spectrum of a signal is difficult. To solve this, we leverage the analytic transformation of a signal using the Hilbert Transform. The key advantages of this technique are maintaining global temporal dependencies and magnitude spectrum, no exploration of design parameters and being extendible to non-stationary and periodic time series.

Lets walk through a simple example for a signal, $\mathbf{x}(t) = 2\cos(w_0t)$ which can be written in the polar coordinates as $\mathbf{x}(t) = e^{iw_0t} + e^{-iw_0t}$. Applying the HT conditions from Equation 4, $\text{HT}(\mathbf{x}(t)) = 2\sin(w_0t)$. Essentially, HT shifts the signal by $\pi/2$ radians. We conduct this instance-level augmentation for each variate of the time series input. The aim is to diversify the phase representation. We use the *scipy* (Virtanen et al., 2020) library to implement this augmentation.

STFT specifications : Non-stationary signals contain time-varying spectral properties. We use STFT to capture these magnitude and phase responses in both time and frequency domains. There are three main arguments to compute STFT - length of each segment (characterized by the window size and the ratio for overlap), the number of frequency bins, and the sampling rate. We use the *scipy* library to implement this operation and use a $k < 1$ as a multiplier to the length of the window W to give the segment length as $k \times W$ with no overlap between segments. The complete list of STFT specifications is given in Table 6. We also demonstrate a sensitivity analysis concerning the number of frequency bins and the segment length in Figure 5.

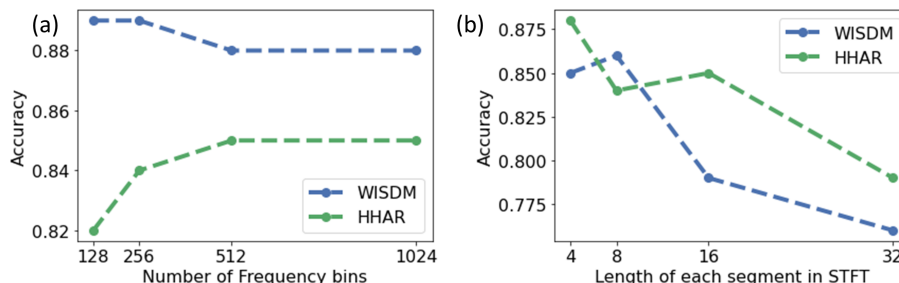


Figure 5. Illustration of the sensitivity of performance to the design choices of STFT by varying a) the number of frequency bins with a fixed segment length of 4 and b) by varying the segment lengths with a 1024 frequency bins.

Table 6. Arguments for STFT computation

Dataset	Sampling Rate	Sequence Length	STFT segment length	Number of frequency bins
WISDM	20 Hz	128	4	1024
HHAR	100 Hz	128	4	1024
UCIHAR	50 Hz	128	4	1024
SSC	100 Hz	3000	16	1024
GR	200 Hz	200	4	1024

Note: It is tempting to use an empirical mode transformation and then apply a Hilbert-Huang transformation to obtain an instantaneous phase and amplitude response in the case of non-stationary signals. It absolves us from a finite time-frequency resolution for the STFT spectra. However, our initial results indicate a high dependence on the choice of the number of

intrinsic mode functions (Huang, 2014) for signal decomposition. Hence, for a generalizable approach, we choose STFT as the tool for the time-frequency spectrum.

Backbones for Temporal Encoder The choice of temporal encoder, F_{Tem} , is not central to our design. Table 7 demonstrates the performance of PhASER under the identical settings for four cross-person settings using WISDM datasets using different backbones for F_{Tem} . For the convolution-based self-attention (second row in Table 7) we use three encoders to compute query (W_q), key (W_k), and value (V) matrices for \mathbf{r}_{Dep} following the guidelines from Vaswani et al. (2017). Then we compute self-attention as, $A = \text{softmax}\left(\frac{QK^T}{\sqrt{d_k}}\right)V$, where d_k is the temporal dimension of \mathbf{r}_{Dep} . Subsequently, we use $\hat{\mathbf{r}}_{\text{Dep}} = \mathbf{r}_{\text{Dep}} + A$, as the input to F_{Tem} . For more details on the convolution and transformer backbones refer to Section D.3.

Table 7. Results for 4 different cross-person settings for WISDM dataset.

Backbones for F_{Tem}	1	2	3	4
2D Convolution based	0.86	0.85	0.86	0.84
2D Convolution based with self-attention	0.88	0.83	0.84	0.81
Transformer	0.87	0.84	0.87	0.84

C. Dataset Details

Past works (Gagnon-Audet et al., 2022; Ragab et al., 2023a) have shown that the datasets used in our work suffer from a distribution shift across users and also within the same user temporally. This makes them suitable for evaluating the efficacy of our framework. In this section, we provide more details on the datasets. Table 8 summarizes the average ADF statistics of the datasets along with their variates and their number of classes and domains.

Table 8. Summary of the dataset attributes. Higher value of ADF stat indicates greater non-stationarity within a signal.

Category	Dataset	Representative ADF-Statistic (mean across all variates)	Variates	Domains	Classes
Human Activity recognition	UCIHAR	-2.58	9	31	6
Human Activity recognition	HHAR	-1.74	3	9	6
Human Activity recognition	WISDM	-0.78	3	36	6
Gesture Recognition	EMG	-33.14	8	36	6
Sleep Stage Classification	EEG	-3.7	1	20	5

WISDM (Kwapisz et al., 2011): It originally consists of 51 subjects performing 18 activities but we follow the ADA-Time (Ragab et al., 2023a) suite to utilize 36 subjects comprising of 6 activity classes given as walking, climbing upstairs, climbing downstairs, sitting, standing, and lying down. The dataset consists of 3-axis accelerometer measurements sampled at 20 Hz to predict the activity of each participant for a segment of 128-time steps. According to Ragab et al. (2023a), this is the most challenging dataset suffering from the highest degree of class imbalance.

HHAR (Stisen et al., 2015): To remain consistent with the existing AdaTime benchmark we leverage the Samsung Galaxy recordings of this dataset from 9 participants from a 3-axis accelerometer sampled at 100 Hz. The 6 activity classes, in this case, are - biking, sitting, standing, walking, climbing up the stairs, and climbing down the stairs.

UCIHAR (Bulbul et al., 2018): This dataset is collected from 30 participants using 9-axis inertial motion unit using a waist-mounted cellular device sampled at 50 Hz. The six activity classes are the same as WISDM dataset.

SSC (Goldberger et al., 2000): This is a single channel EEG dataset collected from 20 subjects to classify five sleep stages - wake, non-rapid eye movement stages - N1, N2, N3, and rapid-eye-movement.

GR (Lobov et al., 2018): For surface-EMG based gesture recognition we follow Lu et al. (2023)’s preprocessing and use an 8-channel data recorded from 36 participants for six types of gestures sampled at 200 Hz.

D. Implementation Details

All experiments are performed on an Ubuntu OS server equipped with NVIDIA TITAN RTX GPU cards using PyTorch framework. Every experiment is carried out with 3 different seeds (2711, 2712, 2713). During model training, we use Adam optimizer (Kingma et al., 2020) with a learning rate from 1e-5 to 1e-3 and maximum number of epochs is set to 150 based on the suitability of each setting. We tune these optimization-related hyperparameters for each setting and save the best model checkpoint based on early exit based on the minimum value of the loss function achieved on the validation set.

D.1. Dataset Configuration

There is no established baseline for domain generalization for time-series where the domain labels and target samples are inaccessible. We leverage past works of Ragab et al. (2023a); Lu et al. (2023) for preprocessing steps. For each dataset we use a cross-person setting in four scenarios. The details of the target domains chosen in each scenario are given in Table 9, the rest are used as source domains. Note for GR we use the same splits as Lu et al. (2023). Our method is not influenced by domain labels as we do not require them for our optimization.

Table 9. Target domain splits for 4 scenarios of each dataset.

Target Domains	Scenario 1	Scenario 2	Scenario 3	Scenario 4
WISDM	0-9	10-17	18-27	28-35
HHAR	0,1	2,3	4,5	6-8
UCIHAR	0-7	8-15	16-23	24-29
GR	0-8	9-17	18-26	27-35
SSC	0-5	5-9	10-14	15-20

D.2. Baseline Methods

General Domain Generalization Methods. For all the standard domain generalization baselines we use conv2D layers for feature transformation of multivariate time series. It is worth mentioning that DANN is actually a domain adaptation study, which requires access to certain unlabeled target domain data. For cross-person generalization, the source domain consists of data from multiple people, in which we divide the source domain data into two parts with equal size and view one of them as the target domain to leverage DANN for domain-invariant training. As for one-person-to-another cases, we randomly sample a small number of unlabeled instances from each target person and merge them into the target set that is needed for running DANN.

BCResNet. This is a competitive benchmark for several audio-scene recognition challenges and demonstrates many useful techniques for domain generalization. BCResNet originally required mel-frequency-cepstral-coefficients but it is not suitable for time-series, hence, we use standard STFT of the multivariate-time series as input in this case.

Non-Stationary Transformer. This is a forecasting baseline that particularly addresses non-stationarity in short-term time sequences, Non-stationary transformer (NSTrans) (Liu et al., 2022b). To adapt it to our setting we use the encoder part of NSTrans followed by a classification head composed of fully connected layers. We simply average the encoder’s output from all time steps and feed it to this classifier head.

Ours+RevIN. Further, we demonstrate that statistical techniques like Reversible Instance Normalization (RevIN) (Kim et al., 2021c) may be used as a plug-and-play module with our framework. One limitation of using RevIN is that the input and output dimensions of this module must have the same dimensions to de-normalize the instance in the feature space. This may limit the usability of the module, however, we find that applying this module around the fusion encoder specifying the same number of input and output channels in the 2D convolution layer is suitable. We do not observe any significant benefit of incorporating this module from the experiments, however, if an application can specifically benefit from such RevIN, PhASER framework can support it.

Diversify. The goal of this design is to characterize the latent domains and use a proxy-training schema to assign pseudo-domain labels to the samples to learn generalizable representations. It is an end-to-end version of the adaptive RNN (Du et al., 2021) method which also proposes to identify sub-domains within a domain for generalization. It is interesting to note that for time-series generalizable representation viewing the non-stationarity or intra-domain shifts is crucial. Both

diversify and PhASER address this problem from completely different approaches and demonstrate improvement over other standard methods or even domain adaptation methods that have the advantage of accessing samples from unseen distributions. While diversify aims to characterize latent distributions and uses a parametric setting, PhASER forces the model to learn domain-invariant features by anchoring the design to the phase which is intricately tied to non-stationarity. It also highlights that time-series domain generalization is a unique problem (compared to the more popular visual domain) and dedicated frameworks need to be designed in this case.

MAPU. MAPU is the state-of-the-art source-free domain adaptation study for time series, thus, in fact, it does not apply to the time-series domain generalizable learning problem. However, we still view it as an effective approach that can address distribution shifts and achieve domain-invariant learning. In our implementation, in addition to the source domain data, we still provide MAPU with the unlabeled target domain data for both cross-person generalization and one-person-to-another cases. The training procedure is identical to the default MAPU design, which is to pre-train the model on labeled source domain data and then conduct the training on unlabeled target domain data.

Table 10. Complete set of results from three trials on each baseline for WISDM cross-person generalization setting.

Baselines	Scenario 1		Scenario 2		Scenario 3		Scenario 4	
	Mean	Std	Mean	Std	Mean	Std	Mean	Std
ERM	0.57	0.02	0.50	0.02	0.51	0.02	0.55	0.02
GroupDRO	0.71	0.06	0.67	0.06	0.60	0.07	0.67	0.04
DANN	0.71	0.02	0.65	0.01	0.65	0.06	0.70	0.03
RSC	0.69	0.05	0.71	0.07	0.64	0.10	0.61	0.11
ANDMask	0.74	0.01	0.73	0.03	0.69	0.06	0.69	0.03
BCResNet	0.83	0.00	0.79	0.04	0.75	0.04	0.78	0.04
NSTrans	0.43	0.02	0.40	0.01	0.37	0.02	0.37	0.03
MAPU	0.75	0.02	0.69	0.04	0.79	0.06	0.79	0.03
Diversify	0.82	0.01	0.82	0.01	0.84	0.01	0.81	0.01
Ours + RevIN*	0.86	0.01	0.85	0.01	0.84	0	0.84	0.03
Ours	0.86	0.01	0.85	0.01	0.85	0.01	0.82	0.02

Table 11. Complete set of results from three trials on each baseline for HHAR cross-person generalization setting.

Baselines	Scenario 1		Scenario 2		Scenario 3		Scenario 4	
	Mean	Std	Mean	Std	Mean	Std	Mean	Std
ERM	0.49	0.05	0.46	0.01	0.45	0.02	0.47	0.03
GroupDRO	0.60	0.01	0.53	0.02	0.59	0.02	0.64	0.03
DANN	0.66	0.01	0.71	0.01	0.67	0.09	0.69	0.03
RSC	0.52	0.05	0.49	0.04	0.44	0.03	0.47	0.03
ANDMask	0.63	0.02	0.64	0.06	0.66	0.11	0.69	0.05
BCResNet	0.66	0.05	0.70	0.06	0.75	0.04	0.68	0.04
NSTrans	0.21	0.02	0.22	0.03	0.27	0.04	0.28	0.02
MAPU	0.73	0.02	0.72	0.03	0.81	0.01	0.78	0.03
Diversify	0.82	0.01	0.76	0.01	0.82	0.01	0.68	0.01
Ours + RevIN*	0.82	0.05	0.82	0.02	0.92	0.04	0.85	0.03
Ours	0.83	0.02	0.83	0.02	0.94	0.03	0.88	0.02

D.3. Implementation Details of PhASER

The magnitude and phase encoders, F_{Mag} and F_{Pha} are implemented using 2D convolution layers with the number of input channels equal to the variates, V , and the out channels as $2c$ with (5×5) kernels. c is a hyperparameter used to conveniently control the size of the overall network. For all HAR and GR models we adopt c as 1 and for SSC c is 4. For more specific details please refer to our code. The sub-spectral feature normalization uses a group number of 3 and follows Equation 2.3 for operation. This is inspired by Chang et. al (Chang et al., 2021) subspectral normalization for audio applications with a frequency spectrum input. The key idea is to conduct sub-band normalization (across a fixed set of frequency bins along time and examples for each channel). We find merit in using this technique for domain generalizable applications, as it can help overcome the low-frequency drifts arising due to device differences (for eg. DC drifts in various sensors). One

Table 12. Complete set of results from three trials on each baseline for UCIHAR cross-person generalization setting.

Baselines	Scenario 1		Scenario 2		Scenario 3		Scenario 4	
	Mean	Std	Mean	Std	Mean	Std	Mean	Std
ERM	0.72	0.09	0.64	0.05	0.70	0.01	0.72	0.03
GroupDRO	0.91	0.02	0.84	0.01	0.89	0.04	0.85	0.07
DANN	0.84	0.02	0.79	0.01	0.81	0.02	0.86	0.03
RSC	0.82	0.13	0.73	0.07	0.74	0.03	0.81	0.06
ANDMask	0.86	0.08	0.80	0.06	0.76	0.13	0.78	0.09
BCResNet	0.81	0.02	0.77	0.02	0.78	0.02	0.83	0.02
NSTrans	0.35	0.02	0.35	0.01	0.51	0.02	0.47	0.01
MAPU	0.85	0.03	0.80	0.01	0.85	0.02	0.82	0.03
Diversify	0.89	0.03	0.84	0.04	0.93	0.02	0.90	0.02
Ours + RevIN*	0.96	0.01	0.90	0.01	0.93	0.03	0.97	0.01
Ours	0.96	0.01	0.91	0.01	0.95	0	0.97	0.01

implementation-specific modification we carried out to ensure a generalizable framework is that if the number of sub-bands is not divisible by the total number of features then we choose to apply the remainder bands with batch-normalization. The output from the respective encoders is then fused along the channel/variante axis by multiplying with 2D convolution kernels to provide a new feature map which is the input to our phase-driven residual network. The F_{Fus} similarly is implemented using 2D convolution layers with the number of input channels as $4c$ and output channels to be $2c$.

Subsequently for the depth-wise encoder, F_{Dep} , we use 2D convolution layers with batch normalization and SiLU (Elfwing et al., 2018) activation function. This style of architecture is closely adapted from the basic building blocks in BCResNet (Kim et al., 2021a). After average pooling the F_{Tem} can assume any backbone as per the requirements of the application. As demonstrated previously in Section B, the choice of backbone is not central to our design here. We find that some applications (like WISDM and GR) benefit from attention-based temporal encoding more than others. For the attention-based version of F_{Tem} we used a multi-headed attention based on a transformer encoder (Vaswani et al., 2017). Regarding positional encoding, we used a simple sinusoid-based encoding and added it to the sequence representation \mathbf{r}_{Dep} . However, arriving at the best positional encoding for numerical time-series data is an active area of research (Kazemi et al., 2019; Tang et al., 2023; Mohapatra et al., 2023c) given its uniqueness compared to typical natural language inputs and further optimizations can be carried out. For the the convolution-based F_{Tem} we simply use a kernel of size (1×3) in a 2D convolution layer to conduct temporal convolutions.

For the classification head, g_{Cls} , we apply 2D convolution layers to have the number of output channels equal to the number of classes in an application, followed by softmax operation. Interestingly, if the choice of F_{Tem} remains convolutional the entire network can be implemented in a purely convolutional form allowing applicability to real-time problems. The model sizes across the different datasets range from 40k-100k trainable parameters (based on the number of variates, temporal encoding etc.) which is modest and can be further tuned for resource-constrained applications by adjusting the c parameter.

Table 13. Complete set of results from three trials on each baseline for SSC cross-person generalization setting.

Baselines	Scenario 1		Scenario 2		Scenario 3		Scenario 4	
	Mean	Std	Mean	Std	Mean	Std	Mean	Std
ERM	0.50	0.05	0.46	0.04	0.49	0.02	0.45	0.03
GroupDRO	0.57	0.07	0.56	0.03	0.55	0.05	0.59	0.06
DANN	0.64	0.02	0.63	0.02	0.69	0.03	0.63	0.04
RSC	0.50	0.09	0.48	0.02	0.52	0.07	0.46	0.01
ANDMask	0.55	0.10	0.50	0.09	0.54	0.07	0.57	0.08
BCResNet	0.79	0	0.82	0.01	0.79	0.01	0.81	0
NSTrans	0.43	0.02	0.37	0.04	0.42	0.06	0.35	0.03
MAPU	0.69	0.01	0.68	0.01	0.65	0.03	0.69	0.02
Diversify	0.73	0.03	0.76	0.02	0.68	0.05	0.77	0.02
Ours + RevIN*	0.82	0.01	0.79	0.02	0.78	0.01	0.81	0.01
Ours	0.85	0.01	0.80	0.01	0.79	0.01	0.83	0.01

Table 14. Complete set of results from three trials on each baseline for GR cross-person generalization setting.

Baselines	Scenario 1		Scenario 2		Scenario 3		Scenario 4	
	Mean	Std	Mean	Std	Mean	Std	Mean	Std
ERM	0.45	0.02	0.58	0.03	0.57	0.03	0.54	0.04
GroupDRO	0.53	0.08	0.36	0.11	0.59	0.05	0.45	0.13
DANN	0.60	0.01	0.66	0.04	0.65	0.02	0.64	0.03
RSC	0.50	0.10	0.66	0.05	0.64	0.03	0.56	0.03
ANDMask	0.41	0.13	0.54	0.20	0.45	0.15	0.39	0.12
BCResNet	0.62	0.06	0.67	0.09	0.65	0.05	0.61	0.07
NSTrans	0.31	0.01	0.34	0.01	0.34	0.01	0.32	0.02
MAPU	0.64	0.02	0.69	0.03	0.71	0.01	0.68	0.04
Diversify	0.69	0.01	0.80	0.01	0.76	0.02	0.76	0.01
Ours + RevIN*	0.68	0.03	0.81	0.04	0.77	0.03	0.76	0.02
Ours	0.70	0.02	0.82	0.02	0.77	0.04	0.75	0.01

Table 15. Complete set of results from three trials on each baseline for HHAR one-person-to-another setting.

Baselines	0		1		2		3		4		5		6		7		8	
	Mean	Std	Mean	Std	Mean	Std	Mean	Std	Mean	Std	Mean	Std	Mean	Std	Mean	Std	Mean	Std
ERM	0.27	0.01	0.40	0.05	0.41	0.05	0.44	0.05	0.42	0.08	0.44	0.01	0.45	0.04	0.44	0.04	0.48	0.02
GroupDRO	0.33	0.02	0.53	0.02	0.38	0.05	0.48	0.04	0.47	0.04	0.51	0.08	0.47	0.03	0.48	0.02	0.49	0.05
DANN	0.32	0.03	0.44	0.05	0.42	0.03	0.45	0.06	0.42	0.03	0.48	0.04	0.49	0.02	0.45	0.05	0.51	0.01
RSC	0.27	0.03	0.45	0.06	0.38	0.05	0.45	0.09	0.40	0.08	0.47	0.02	0.50	0.06	0.44	0.08	0.53	0.01
ANDMask	0.34	0.06	0.50	0.03	0.37	0.04	0.43	0.05	0.46	0.04	0.51	0.07	0.46	0.03	0.47	0.02	0.52	0.03
BCResNet	0.28	0.03	0.48	0.08	0.32	0.04	0.47	0.03	0.42	0.06	0.52	0.05	0.44	0.02	0.45	0.02	0.49	0.06
NSTrans	0.20	0.01	0.22	0.02	0.17	0.02	0.20	0.01	0.21	0.01	0.22	0.01	0.26	0.07	0.17	0.05	0.20	0.01
MAPU	0.39	0.05	0.57	0.05	0.35	0.06	0.52	0.03	0.49	0.04	0.54	0.02	0.49	0.01	0.50	0.06	0.52	0.04
Diversify	0.42	0.04	0.62	0.04	0.32	0.09	0.62	0.01	0.56	0.03	0.61	0.01	0.53	0.04	0.52	0.10	0.61	0.05
Ours + RevIN*	0.48	0.02	0.66	0.08	0.57	0.05	0.65	0.03	0.61	0.04	0.64	0.05	0.65	0.06	0.64	0.01	0.63	0.03
Ours	0.53	0.04	0.70	0.03	0.63	0.01	0.66	0.03	0.64	0.06	0.67	0.01	0.65	0.03	0.67	0.04	0.62	0.02

D.4. Ablation Details of PhASER

For row 1 in Table 5, the modification to PhASER is straightforward by simply omitted the Hilbert transformation during data preprocessing. When the separate encoders are not used (rows 6 and 7 in Table 5), we only use F_{Mag} and connect the output of the sub-feature normalization block directly to the F_{Dep} . When the residual is removed entirely (rows 5 and 6 in Table 5), we cannot broadcast the 1D input to 2D anymore so we take the mean across all the temporal indices of $F_{Tem}(r_{Dep})$ and flatten it to input to fully connected layers. Based on the dataset we choose a few fully connected layers truncating to the number of classes finally.

D.5. Phase-driven NSTrans

Non-stationary transformer, NSTrans (Liu et al., 2022c), applies a destationarizing attention around the transformer block. Since it is typically used for forecasting tasks, it comprises of encoder and a decoder module. For adapting this model to classification we update the design to conduct normalization and denormalization around the encoder block. We use this modified version of NSTrans as the F_{Tem} module in PhASER and observe significant improvement in performance as shown in Figure 4.

E. Supplementary of Main Results

We conduct all experiments with three random seeds (2711, 2712, 2713), and present the error range in this section. Tables 10, 11 and 12 represent the mean and standard deviation corresponding to the main paper’s Table 2 for the WISDM, HHAR and UCIHAR datasets respectively. Tables 13 and 14 are the complete representations of all the runs corresponding to Table 4 in the main paper for sleep stage classification and gesture recognition respectively. Table 15 corresponds to the Table 3 in the main paper for the complete performance statistics for one person to another generalization using HHAR dataset.